Expression, Purification, and Crystallization of Recombinant Human ABL1 Kinase Domain for X-ray Crystallography-Based Structural Studies

by

Ayça İrgit

A Dissertation Submitted to the
Graduate School of Sciences and Engineering
in Partial Fulfillment of the Requirements for
the Degree of

Master of Science

in

Molecular Biology and Genetics

July 11, 2025

Expression, Purification, and Crystallization of Recombinant Human ABL1 Kinase Domain for X-ray Crystallography-Based Structural Studies

Koç University

Graduate School of Sciences and Engineering

This is to certify that I have examined this copy of a master's thesis by

Ayça İrgit

and have found that it is complete and satisfactory in all respects,
and that any and all revisions required by the final
examining committee have been made.

Committee Members:

Assist. Prof. Hasan Demirci (Advisor)

Assoc. Prof. Halilibrahim Çiftçi (Co-Advisor)

Assoc. Prof. Belgin Sever

Assist. Prof. Onur Öztaş

Assist. Prof. İsmail Kudret Sağlam

Date: July, 11, 2025

To my dearest ones…

ABSTRACT

Expression, Purification, and Crystallization of Recombinant Human ABL1 Kinase Domain for X-ray Crystallography-Based Structural Studies

Ayça İrgit

Master of Science in Molecular Biology and Genetics

July 11, 2025

The Abelson1 (ABL1) is a member of the Abelson (ABL) non-receptor tyrosine kinase family and is central to the regulation of several cellular processes, such as proliferation, survival, and differentiation. ABL1 is composed of several functionally distinct and structurally specialized domains; including an N-terminal cap region, SH2 and SH3 domains, a bilobed kinase domain, and a C-terminal tail, each playing a role in both regulating kinase activity and participating in complex signaling cascades. Under normal cellular conditions, the ABL1 kinase is found in an inactive state and becomes activated according to cellular needs. The aberrant ABL1 activity is associated with cellular abnormalities and disease pathogenesis including Chronic Myeloid Leukemia (CML). CML is a blood cancer type that is characterized by the constitutively active BCR-ABL1 protein arising from the fusion of *ABL1* with the *Breakpoint Cluster Region (BCR)* gene. The deletion of the regulatory sequences of *ABL1* and the insertion of additional *BCR* fragments leads to the constitutive activation of the BCR-ABL1 protein and oncogenic effects. The central role of ABL1 in the progression of CML, makes it the main target for the treatment approaches. Tyrosine kinase inhibitors (TKIs) targeting ABL1 provide an effective strategy for CML treatment by blocking the oncogenic, constitutive activity arising from the BCR-ABL1 fusion. Despite the success of the TKIs in the management of CML, there is a need for new strategies and treatment approaches to improve the treatment efficiency and outcomes. The structural studies that focus on the enlightening structural features of the ABL1 kinase are crucial for the development of novel TKIs and therapeutic approaches for the effective management of CML. This study focuses on the expression, purification and crystallization of ABL1 kinase for its structural investigations that could contribute to the development of novel therapeutics and drug screening platforms.

ÖZETÇE

X-ışını Kristalografisine Dayalı Yapısal Çalışmalar İçin Rekombinant İnsan ABL1 Kinaz Bölgesinin Ekspresyonu, Saflaştırılması ve Kristallendirilmesi

Ayça İrgit

Moleküler Biyoloji ve Genetik, Yüksek Lisans

11 Temmuz 2025

Abelson1 (ABL1), Abelson (ABL) ailesine ait bir reseptör olmayan tirozin kinazdır ve hücre çoğalması, hayatta kalma ve farklılaşma gibi çeşitli hücresel süreçlerin düzenlenmesinde merkezi bir rol oynar. ABL1, işlevsel olarak farklı ve yapısal olarak özelleşmiş çeşitli bölgelerden oluşur; bu bölgeler arasında N-terminal kapak bölgesi, SH2 ve SH3 domainleri, iki loblu bir kinaz domaini ve C-terminal kuyruk yer alır. Her bir yapı, hem kinaz aktivitesinin düzenlenmesinde hem de karmaşık sinyal iletim yollarına katılımda rol oynar. Normal hücresel koşullarda ABL1 kinaz inaktif (etkin olmayan) durumda bulunur ve hücresel ihtiyaçlara göre aktive edilir. ABL1'in anormal aktivitesi, hücresel bozukluklar ve özellikle Kronik Myeloid Lösemi (CML) olmak üzere çeşitli hastalıkların patogenezinde ilişkilidir. CML, ABL1 geninin Kırılma Noktası Küme Bölgesi (BCR) geni ile birleşmesi sonucu oluşan sürekli aktif BCR-ABL1 proteini ile karakterize edilen bir kan kanseri türüdür. ABL1'in düzenleyici dizilerinin silinmesi ve BCR genine ait ek bölümlerin eklenmesi, BCR-ABL1 proteininin sürekli aktif hale gelmesine ve onkojenik etkilere yol açar. ABL1'in CML gelişimindeki merkezi rolü, onu tedavi yaklaşımlarının ana hedefi haline getirir. ABL1'i hedef alan tirozin kinaz inhibitörleri (TKI'lar), BCR-ABL1 füzyonundan kaynaklanan onkojenik ve sürekli aktiviteyi bloke ederek CML tedavisinde etkili bir strateji sunar. TKI'ların CML yönetimindeki başarısına rağmen, tedavi etkinliğini ve sonuçlarını iyileştirmek için yeni strateji ve tedavi yaklaşımlarına ihtiyaç vardır. ABL1 kinazın yapısal özelliklerini aydınlatmayı amaçlayan yapısal çalışmalar, yeni TKI'ların ve etkili CML tedavileri için terapötik yaklaşımların geliştirilmesinde büyük önem taşır. Bu çalışma, ABL1 kinazın ekspresyonu, saflaştırılması ve kristalizasyonuna odaklanmakta olup, yapısal analizler aracılığıyla yeni tedavi yöntemlerinin ve ilaç tarama platformlarının geliştirilmesine katkı sağlamayı amaçlamaktadır.

AKNOWLEDGEMENTS

I am deeply grateful to Asst. Prof. Hasan Demirci for the opportunity to pursue my Master's studies and research in his laboratory. His contributions and constructive suggestions have greatly enriched my project and helped me grow academically.

I would also like to thank Assoc. Prof. Halilibrahim Çiftçi and Assoc. Prof. Belgin Sever for their valuable support and encouragement throughout my research. Their guidance and encouragement have played an important role in my scientific development.

I am also thankful to the members of my thesis committee, Asst. Prof. Onur Öztaş and Asst. Prof. İsmail Kudret Sağlam, for their time, feedback, and support.

I would like to thank the Turkish Health Institutes (TÜSEB) for the scholarship support provided during my M.Sc. studies under the project titled “Yeni ABL İnhibitörü Oleanolik Asit Türevlerinin Geliştirilmesi” (Project No: 24333).

I would also like to thank the members of KUYBIIG-M for their cooperation, friendship, and creating a positive and supportive working environment. I am especially grateful to my friends Alaleh Shafiei, Bilge Tosun, Cahine Kulakman, Cengiz Kaan Ferah, Ece Akyüz, Edanur Topalan, Haluk Çetinok, İlkin Yapıcı, Necati Atalay, Nilüfer Baldır, Ömür Güven, Seyide Seda Paydos, and Zeliş Nergis for their friendship, kindness and constant support.

Additionally, I would like to thank my intern, Reyhan Kamış, for her dedicated support throughout this project and for being such a great friend. Her commitment, hard work, and valuable contributions greatly enriched the research.

I am deeply grateful to my fiance, Ahmet Celayir, for his love, constant support, and endless patience throughout this journey. His encouragement and belief in me have been a vital source of strength, helping me overcome challenges and stay motivated. Thank you for standing by my side and being my greatest companion.

I would like to express my deepest gratitude to my family, whose unconditional love, support, and encouragement have been the foundation of everything I have achieved. I extend my deepest gratitude to my mother, Mücella; my father, Ali; and my little sister, Eylül. Their belief in me gave me strength during the most challenging times, and their constant presence has been my greatest source of motivation.

TABLE OF CONTENTS

LIST OF TABLES

LIST OF FIGURES

ABBREVIATIONS

ABL	Abelson
ABL1	Abelson1
ABL2	Abelson2
BCR	Breakpoint Cluster Region
CML	Chronic Myeloid Leukemia
D	Aspartate
ddH2O	Deionized distilled water
F	Phenylalanine
G	Glycine
His	Histidine
IPTG	Isopropyl β-D-1-thiogalactopyranoside
kDa	Kilodalton
KD	Kinase Domain
L	Liter
LB	Luria-Bertani
min	Minute
ml	Milliliter
mM	Millimolar
Ni-NTA	Nickel-Nitrilotriacetic Acid
NLS	Nuclear Localization Signal
NRTK	Non-receptor Tyrosine Kinase
OD	Optical Density
PDB	Protein Data Bank
RTK	Receptor Tyrosine Kinase
rpm	Revolutions per Minute
SDS	Sodium Dodecylsulfate
SDS-PAGE	SDS-Polyacrylamide Gel Electrophoresis

SH2	Src homology-2
SH3	Src homology-3
SUMO	Small Ubiquitin-like Modifier
TK	Tyrosine Kinase
TKI	Tyrosine Kinase Inhibitor
ULP1	Ubiquitin-like-specific protease 1
XRD	X-ray Diffractometer
µl	Microliter

Chapter 1

INTRODUCTION

1.1. Tyrosine Kinases

The Tyrosine Kinase (TK) family with more than 90 members regulates the cellular signaling by catalyzing the ATP phosphorylation of the specific tyrosine residue on target protein (Rygiel et al., 2023). By transferring a phosphate group from ATP, they mediate a covalent post-translational modification on the target protein which is essential to maintain homeostasis in the cell (Paul, 2004). In response to intracellular and extracellular stimuli, TKs regulate many of the critical biological processes including cell metabolism, growth, survival, differentiation, cell movement, and apoptosis (Paul et al., 2004).

TKs are classified into 2 subgroups according to their structural organization: receptor tyrosine kinases (RTKs) and non-receptor tyrosine kinases (NRTKs). Despite their structural differences, both families are similar in their function as being key mediators of the signaling cascades in the cell (Eshaq et al., 2024).

RTKs are transmembrane proteins composed of an extracellular ligand-binding domain, a single transmembrane alpha-helix, and a kinase domain which regulates the kinase activation (Paul et al., 2004). RTKs play a central role in cell proliferation and division by activating the signaling cascade in the RAF-MEK-ERK pathway. With more than 50 members, RTKs are the largest subfamily of the TKs (Rygiel et al., 2023). EGFR, PDGFR, FGFR, and the insulin receptor are some well-known members of the RTK family.

1.1.1. Non-Receptor Tyrosine Kinases

NRTKs are found in both nucleus and cytoplasm of the cell, and unlike the RTKs, they lack extracellular and transmembrane domains (Rygiel et al., 2023, Eshaq et al., 2024). NRTKs have a highly conserved kinase domain with distinct structural organization of the N-terminal lobe, and C-terminal lobe. The N-terminal lobe contains an α-helix and five-stranded β-sheet, while the C-terminal lobe is mainly composed of α helices (Paul et al., 2004). In addition to the structural heterogeneity of the kinase domain,

the N-terminal and C-terminal lobes are also different in their functions. The N-terminal lobe acts as the phosphate binding site, and the C-terminal lobe functions as substrate binding (Paul et al., 2004). Between these two lobes, the activation loop which is the main autophosphorylation site for the activation of NRTKs is found. They exist in both active and inactive conformations in the cells and their conformation shifts between these states according to cellular needs (Eshaq et al., 2024). The activation mechanism of NRTKs is complex and requires protein-protein interaction to facilitate transphosphorylation (Paul, 2004).

In addition to the bilobed kinase domain, the majority of the NRTKs include regulatory domains involved in signal transduction or protein-protein interactions, such as SH2 and SH3 (Eshaq et al., 2024). Even though they share a highly conserved kinase domain and structural organization, the NRTKs are classified into different subfamilies according to the kinase domain amino acid variations and sequence similarity (Siveen et al., 2018, Eshaq et al., 2024). The subgroups of the NRTK family are Ack, Jak, Fes, Fak, Tec, Src, Csk, Abl, and Syk kinase families (Siveen et al., 2018, Eshaq et al., 2024).

1.1.2. Abelson Non-Receptor Tyrosine Kinase Family

The Abelson (ABL) family belongs to the NRTK family and includes two members: ABL1 and ABL2 (also known as Abl-related gene or Arg) (Siveen et al., 2018, Guitterez et al., 2023). Both members of the ABL family have a broad range of expression in all tissues whereas the spleen, thymus, and testes have the highest expression level (Eshaq et al., 2024). In several cellular processes including cell growth, survival, and differentiation, response to cellular stress, and cytoskeletal reorganization; ABL kinases play significant roles (Siveen et al., 2018).

The structural features of the ABL kinase family show a high similarity with the NRTK family. Within the ABL family itself, the structural organization is highly conserved with more than %90 sequence identity of ABL1 and ABL2 (Siveen et al., 2018).

1.2. Abelson1

ABL1 is composed of several functionally distinct and structurally specialized domains and motifs. In addition to the highly conserved domains among the NRTK

family, ABL1 also contains more characteristic regions and motifs. The structural features of ABL1 include an N-terminal cap region, Src homology-2 (SH2) and Src homology-3 (SH3) domains, a kinase domain (KD) also known as the SH1 domain, a long tail at the C-terminus including DNA binding domain, actin-binding domain, and signals for nuclear localization, and nuclear export (Figure 1.1). Each domain has a crucial role in the regulation of the kinase activity and overall function of ABL1 (Irgit et al., 2025).

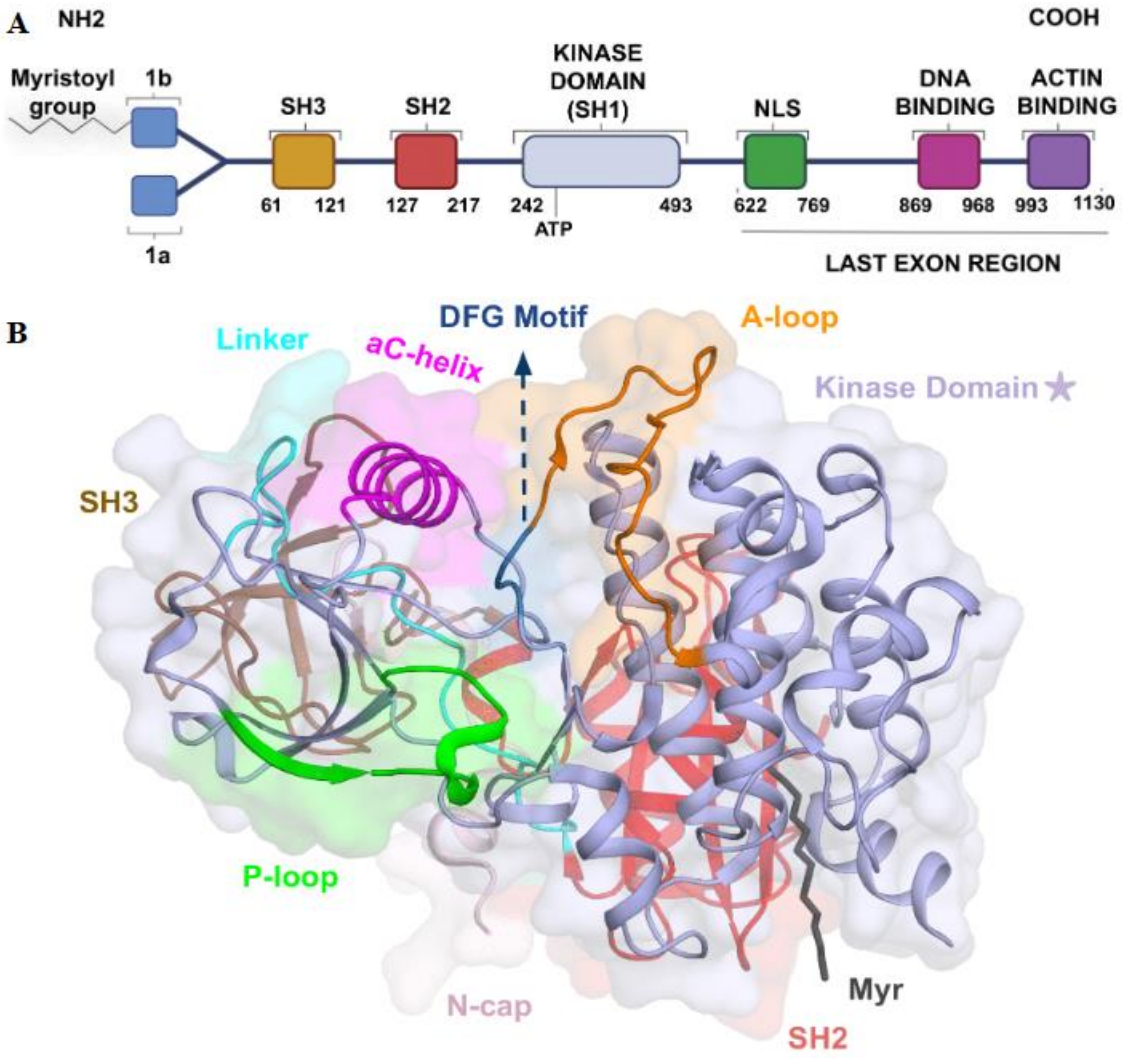

Figure1.1: Structural representation of ABL1. (a) Domain architecture of ABL1. Created via BioRender. (b) Crystal structure of ABL1 (1b) core in the inactive conformation (PDB: 2FO0).

Depending on the myristoylation of its N-terminus, ABL1 kinase exists in two isoforms: 1a without a myristoyl group, and 1b a myristoyl group—a 14-carbon fatty acid

attached (Figure 1.1-a) (Hanstchel et al., 2003). The myristoyl group in 1b isoform plays a role in the autoinhibition of protein by interacting with hydrophobic residues within the kinase domain and forming a hydrophobic pocket that stabilizes the protein in the inactive conformation (Wu et al., 2024).

The C-terminus of ABL1 which is also called the last exon region has specialized regions allowing it to bind DNA and both G-actin and F-actin. In addition, the C-terminus includes three nuclear localization signals and one nuclear export signal (Siveen et al., 2018) which are critical for moving the protein between the nucleus and cytoplasm and are involved in a wide range of signaling pathways that help maintain cellular balance and respond to environmental changes (Irgit et al., 2025). Under physiological conditions, ABL1 is found in both compartments allowing it to regulate distinct signaling pathways and cellular functions.

Like other members of the NRTK family, ABL1 kinase presents in both active and inactive states, and depending on the cellular requirements, their conformation dynamically shifts. Its activity is highly regulated by internal and external molecular interactions. The main regulatory mechanism is the autoinhibition mediated by SH2 and SH3 domains. These domains together stabilize the inactive kinase conformation by forming a clamp structure via hydrophobic interactions (Irgit et al., 2025).

1.2.1. ABL1 Kinase Domain

The ABL1 KD shares the structural characteristics of the NRTK family. It consists of 2 structurally and functionally distinct lobes which are N-lobe and C-lobe, and an activation loop (A-loop) positioned between these two lobes (Wu et al., 2024). The N-lobe is composed of a single α-helix called αC helix five-stranded antiparallel β-sheets. αC helix is a flexible structural element that is critical for the transition between the active and inactive conformations of the kinase. The first two antiparallel β-sheet strands are linked by a glycine-rich phosphate-binding loop (P-loop) that enables the catalytic activity of the kinase and enhances the ATP interaction (Zhang et al., 2022). Meanwhile, the C-terminal lobe serves as the binding site for substrates. A-loop by controlling access to the ATP-binding site is the key regulator of the kinase activity. A-loop contains the Tyr412 residue which is the main autophosphorylation site for the kinase activation. Another key structural element of the A-loop is the conserved aspartate-phenylalanine-

glycine (DFG) motif which is crucial to determining the conformation of the ABL1 (Krishan et al., 2022).

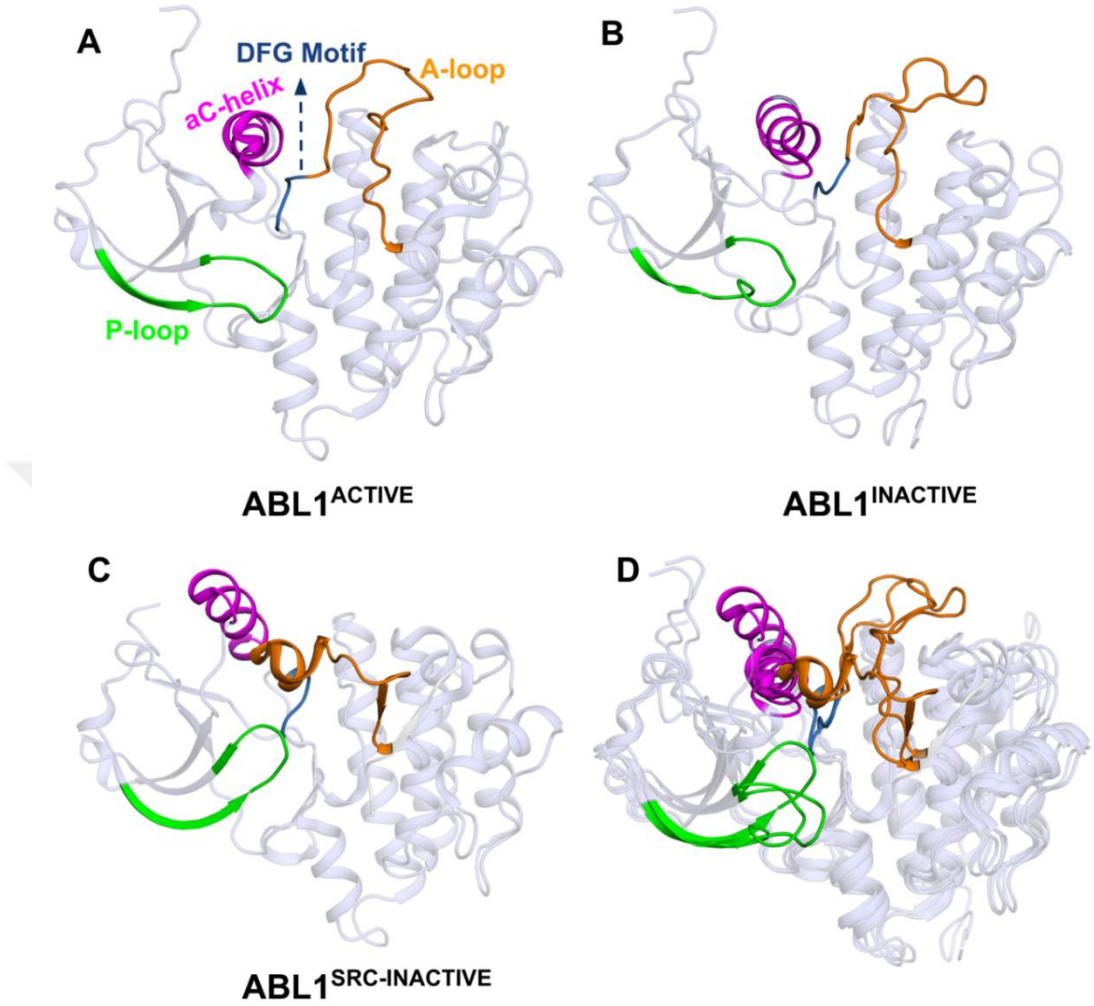

Figure 1. 2: ABL1 kinase domain in different conformations. (A) ABL1 in active (DFG-in) conformation ($ABL1^{ACTIVE}$, PDB: 6XR6). (B) ABL1 in inactive (DFG-out) conformation ($ABL1^{INACTIVE}$, PDB: 6XR7). (C) ABL1 in Src-inactive conformation ($ABL1^{SCR\text{-}INACTIVE}$, PDB: 2G1T). (D) The superposition of the active, inactive, and src-inactive conformations of ABL1 kinase domain.

When ABL1 kinase becomes activated, it undergoes significant conformational changes in the structural elements of the N-lobe and the A-loop (Figure 1.2). In the active conformation of ABL1, the P-loop became more extended which facilitates the ATP binding. Both the αC-helix and A-loop shift into an open/ in conformation that enables the ATP interaction (Figure 1.2-a) (Krishan et al., 2022). The aspartate and phenylalanine residues in the DFG motif plays a crucial role in switching kinase to its active

conformation by interacting with Mg^{2+} and hydrophobic residues respectively. The interaction of the aspartate residue with Mg^{2+} enhances the ATP binding, meanwhile, the hydrophobic pocket formed by interactions between the phenylalanine and other hydrophobic residues helps to stabilize the kinase in its active conformation (Hari et al., 2014, Wu, 2024). In contrast, in the inactive conformation, these structural elements are reoriented to lock the kinase in an inactive state (Figure 1.2-b). The P-loop becomes more compact and both the αC-helix and A-loop adopt a closed/ out conformation that blocks the access of ATP to its binding pocket (Roskoski et al., 2022, Wu et al., 2024).

Besides active and inactive conformations of ABL1, also it can exist in a third, intermediate conformation which is also referred to as Src-like inactive conformation (Figure 1.2-c) due to its similarity to the inactive kinase conformation of c-Src NRTK. In this conformation, A-loop is found in a compact form that prevents the access of ATP whereas αC-helix shifts into the active site supporting the ATP binding and DFG-in position (Levinson et al., 2016).

The kinase activity of ABL1 is highly flexible and strictly controlled to inhibit dysregulations. It is known that the aberrant ABL1 kinase activity is associated with various cellular abnormalities and disease pathogenesis including chronic myeloid leukemia (CML) (El-Tanani et al., 2024).

1.3. Chronic Myeloid Leukemia

CML is a blood cancer type which is defined by the excessive production of immature white blood cells in the bone marrow. With an incidence rate of 2 cases per 100,000 people yearly, CML is classified as a rare leukemia type. Approximately 15% of new leukemia diagnoses in adults are CML (Jabbour et al., 2024).

CML is classified as a myeloproliferative disorder and usually progresses through three phases: chronic phase (CP), accelerated phase (AP), and blast crisis (BC) (Minciacchi, 2021). The progression of the disease is determined by the increasing number of immature blood cells known as blasts. Above %90 of CML patients present in CP. Anemia and splenomegaly are the most common symptoms of CP. Other symptoms of the CP include fever, fatigue, weight loss, left upper quadrant fullness, or pain (Jabbour et al., 2024). As the disease progresses to the BC phase, symptoms may become more serious like bone pain and bleeding.

Most of the patients are diagnosed during the CP, often with few or no symptoms whereas nearly half are diagnosed by chance during routine blood tests (Sampaio et al., 2021). The molecular diagnosis of CML mainly relies on the presence of the Philadelphia chromosome (Charles et al., 1999).

1.3.1. The BCR-ABL1 in Progression of CML

BCR-ABL1 fusion protein arises from the reciprocal translocation between the ABL1 gene on chromosome 9 and the BCR gene on chromosome 22 t(9;22)(q34;q11) in bone marrow cells (Figure 1.3). The resulting chimeric chromosome is referred to as the Philadelphia chromosome and transcribes the oncogenic BCR-ABL1 fusion protein (El-Tanani et al., 2024. Depending on the localization of the breakpoint site in the BCR gene, there are different isoforms of BCR-ABL1 fusion protein p190, p210, and p230. The fused part of the ABL1 is the same in all isoforms whereas the size of the fused BCR fragments varies between the isoforms. The oncogenic activity of the fusion protein varies between the different isoforms and according to the size of fused BCR fragments. The higher oncogenic property of p190 isoform than p230 isoform shows the effect of BCR fragment size in the regulation of the kinase activity and disease progression. Among all isoforms, p210 isoform is central to the CML progression (Charles et al., 1999).

In the BCR-ABL1 fusion protein, when compared to ABL1, there are additional sequences including the coiled-coil domain, Serine–Threonine kinase domain, and Rho/GEF domains that are coming from the BCR gene (Figure 1.3). These additional sequences lead to constitutive activation of the BCR-ABL1 fusion protein. The fusion of the coiled-coil domain of the BCR protein promotes the dimerization and oligomerization of the BCR-ABL1 fusion protein. This oligomerization leads to constitutive kinase activity and promotes the oncogenic effects (Deninger et al., 2000).

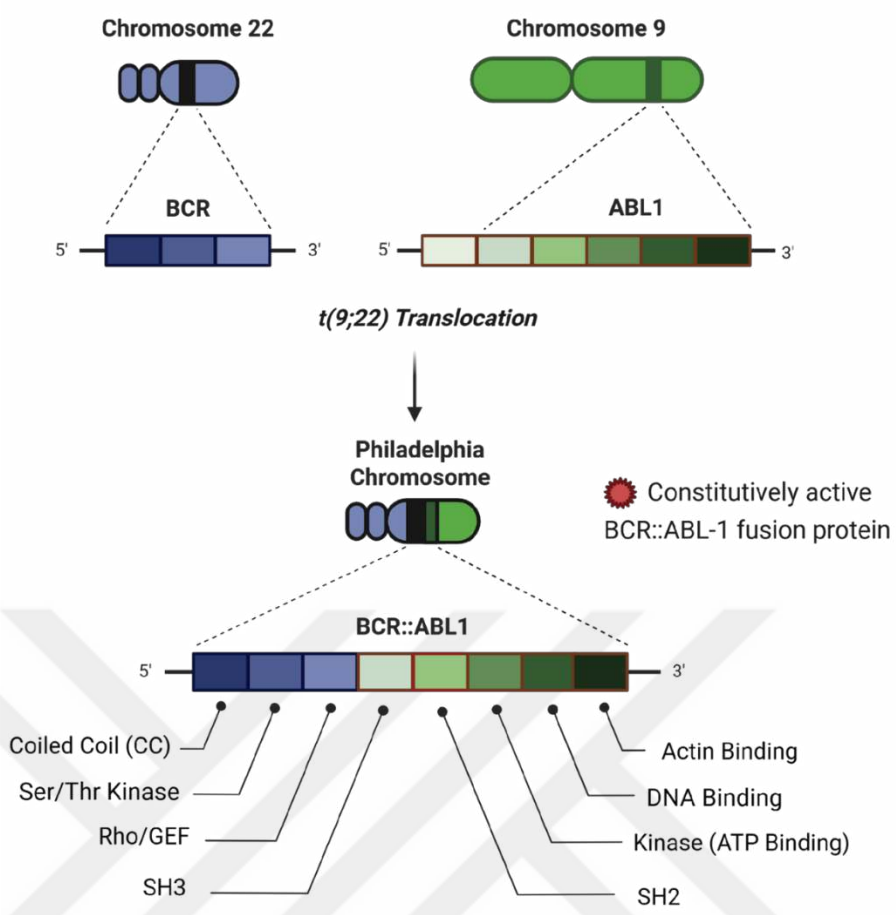

Figure 1.3: The schematic representation of BCR-ABL translocation. Created via BioRender.

In addition to the fusion of additional domains, some of the regulatory domains of ABL1 including N-terminal cap region and C-terminal motifs are deleted in the BCR-ABL1 fusion protein (Figure 1.3). The deletion of the N-terminal cap region disrupts the ABL1's autoinhibition and results in constitutive activation of the protein (Wu et al., 2024). The deletion of the regulatory domains in the C-terminal has significant effects on both the function and localization of the BCR-ABL1 fusion protein (Irgit et al., 2025).

1.3.2. TKIs in CML Treatment

Tyrosine kinase inhibitors (TKIs) by blocking the abnormal activity of the BCR-ABL1 provide an effective strategy for the management of CML. As a result of the inhibition of constitutive activity, TKI blocks the progression of the disease and also

improves long-term patient outcomes and life quality. With the use of TKIs in CML treatment, the mortality rates decreased to 1%–2% from 10%–20% (Jabbour et al., 2024).

Currently, for the treatment of CML six TKIs which are imatinib, nilotinib, dasatinib, bosutinib, ponatinib, and asciminib have received FDA approval (Table 1.1). Based on their mode of action these inhibitors are classified into three generations which are the first-generation, second-generation, and third-generation TKIs (Wu et al., 2024).

Table 1.1: FDA-approved BCR-ABL1 TKIs.

FDA-approved BCR-ABL1 TKIs	FDA Approval Year	Generation	Inhibitory Mode of Action	BCR-ABL1 kinase binding conformation
Imatinib	2001	1st Generation	ATP-competitive	Inactive
Dasatinib	2006	2nd Generation	ATP-competitive	Active
Nilotinib	2007	2nd Generation	ATP-competitive	Inactive
Bosutinib	2012	2nd Generation	ATP-competitive	Both
Ponatinib	2012	3rd Generation	ATP-competitive	Inactive
Asciminib	2021	3rd Generation	Allosteric Inhibitor	Myristoyl pocket

The first generation of TKI includes Imatinib which is the first TKI approved by the FDA for cancer treatment, specifically for CML. It functions as a competitive inhibitor and binds to the ATP-binding pocket of the ABL1 when it is in inactive conformation

(Figure 1.4-b). Imatinib interacts with the ATP pocket through van der Waals interactions and also hydrogen bonding. Even though its success in the management of CML, over time, some patients developed resistance to imatinib. The developed resistance against imatinib and also its ineffectiveness in patients that have ABL1 mutations leads to the development of further TKIs (Sacha et al., 2014, Shoukier et al., 2021). In addition to the inhibitory function of imatinib, recent studies from 2022 have demonstrated its binding to the myristoyl pocket of BCR-ABL1, leading to allosteric activation of the kinase domain (Figure 1.4-c)(Xie etal., 2022).

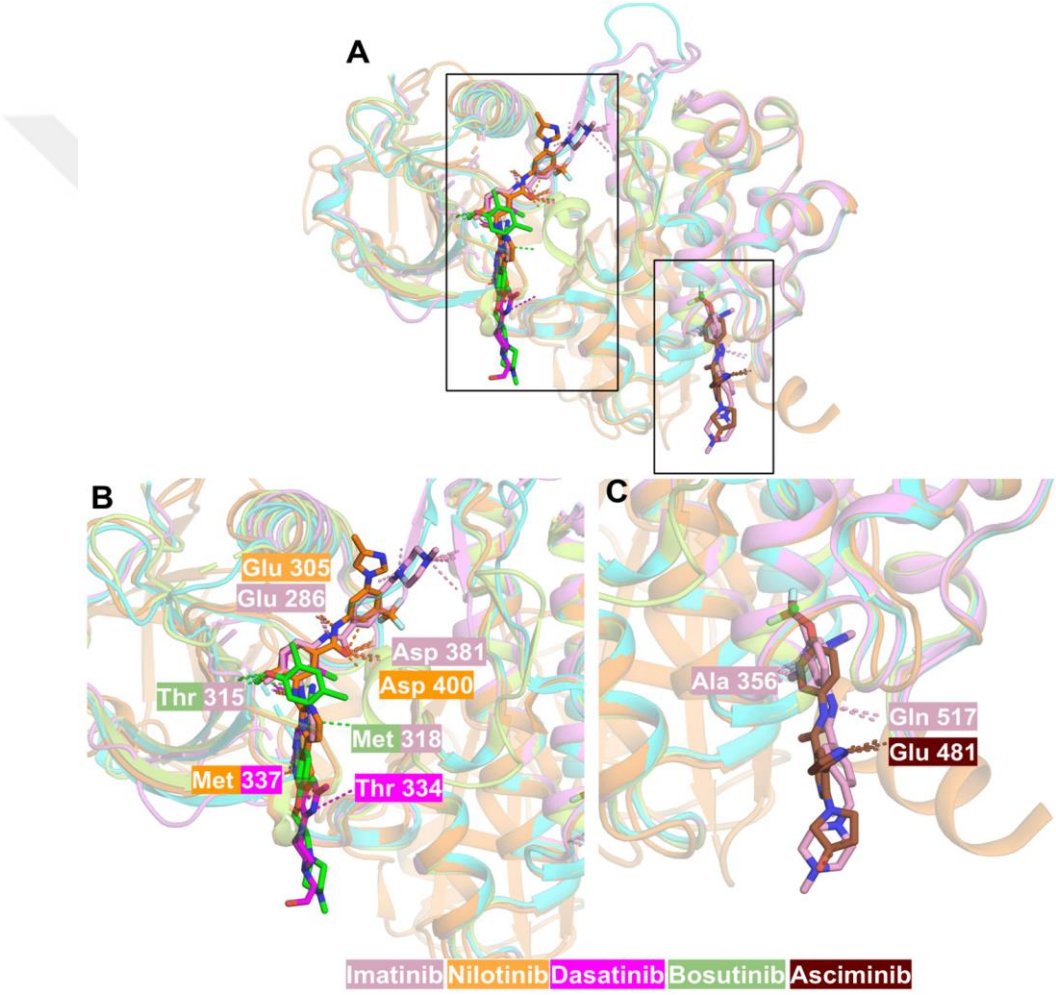

Figure 1.4: The binding mechanisms of TKIs to BCR-ABL1. (A) The superposition of the binding mechanisms of imatinib (pink), nilotinib (orange), dasatinib (magenta), bosutinib (green), and asciminib (brown) to the BCR-ABL1. (B) The interaction between BCR-ABL1 kinase and the TKIs imatinib (yellow), nilotinib (orange), dasatinib (magenta), and bosutinib (green). (C) The interaction between BCR-ABL1 kinase and the TKIs imatinib (pink) and asciminib (brown).

The second-generation TKIs Nilotinib, Dasatinib, and Bosutinib are likely imatinib competitive inhibitors that bind to the ATP pocket and block the access of ATP. Nilotinib binds to the ATP pocket when the ABL1 is in inactive conformation whereas Dasatinib binds when the kinase is in active conformation (Figure 1.4-b) (Oruganti et al., 2022). Bosutinib has a broader activity range and can bind to the ATP pocket (Figure 1.4-b) both in active and inactive conformations of the ABL1 (Levinson et al., 2012). The second-generation TKIs bind to the ATP pocket with extended numbers of van der Waals interactions, and also they are effective against most of the mutations that imatinib remains ineffective (Wu et al., 2024).

Ponatinib and asciminib are the third-generation TKIs. Ponatinib, like the previous TKIs, is a competitive inhibitor that binds to the ATP pocket in the inactive conformation. It is effective against most of the ABL1 mutations including T315I (Tanneeru et al., 2013). Different from the previous TKIs, asciminib is an allosteric TKI binding to the myristoyl pocket of ABL1 (Figure 1.4-c) rather than the ATP pocket. Upon binding of asciminib to the myristoyl pocket, ABL1 undergoes conformational rearrangements that lock the kinase in the inactive form (Shoukier et al., 2021).

Despite their success in management of the CML, current TKIs remain ineffective against certain ABL1 kinase mutations. Additionally, some patients develop resistance to TKIs over time. These limitations emphasize the need for novel TKIs to overcome resistance and enhance therapeutic efficacy (Irgit et al., 2025).

1.4. X-ray Crystallography

For the three-dimensional structure determination of the biomacromolecules at atomic resolution, several techniques including nuclear magnetic resonance (NMR), cryo-electron microscopy, and X-ray crystallography exist. Among these techniques, X-ray crystallography with providing detailed and high-resolution structural information at atomic resolution level is the most commonly used method (Smyth and Martin, 2000). The structure determination of the protein via X-ray crystallography includes main steps which are protein crystal formation; collection of proteins' diffraction patterns by exposing them to X-rays; followed by the data processing via phase determination, electron density map calculation, built of an atomic model, and the validation of the final structure (Mishra et al., 2012).

In the X-ray crystallography-based structure determination, protein crystallization is one of the most challenging steps, often serving as a bottleneck. Several biochemical and biophysical factors influence crystal nucleation and packing by affecting the diffraction quality. Among these factors, protein quality, which is determined by the purity, concentration, solubility, homogeneity, and structural stability, has a primary role in the formation of high-quality crystals (Chayen and Saridakis, 2008; Holcomb et al., 2017). To achieve a high level of protein purity, proteins are mainly subjected to purification via chromatographic method including affinity chromatography, ion-exchange chromatography, and size-exclusion chromatography (Giegé et al., 1995; McPherson and Gavira, 2014). In addition to the protein purity, its concentration is another critical factor that enhances the crystal quality. Both in low and high protein concentrations, the formation of the high-quality crystals and the collection of the diffraction pattern is unlikely (Weber, 1991).

Another important challenge is the maintaining a balance between protein solubility and supersaturation where the excessively soluble proteins resist nucleation, whereas insufficiently soluble proteins tend to aggregation or precipitation. Furthermore, proteins frequently contain flexible loops, disordered regions, or unstable domains that introduce conformational heterogeneity and disrupt the formation of a repetitive, ordered crystal lattice (Holcomb et al., 2017).

Moreover, the protein homogeneity and stability plays a critical role for the success of the crystallization. Even minor heterogeneities in the protein structure such as the presence of multiple oligomeric states, or slight variations in post-translational modifications can dramatically reduce the crystal formation or result in poorly ordered crystals unsuitable for diffraction (Holcomb et al., 2017).

Additionally, by providing the required environmental conditions including pH, precipitant type, and salt concentration, for proteins to undergo nucleation, screening conditions are essential components of the crystallization trials (Weber, 1991).

1.5. Motivation and Aim

The developed resistance against current TKIs emphasizes the need for the development of novel and more effective TKIs and treatment approaches for CML. Structural studies aiming to enlighten the structural features of ABL1 play a fundamental role in the design and development of new TKIs by providing atomic-level knowledge of

the protein's structural characteristics and potential interaction sites. Additionally, these studies offer critical insights into the molecular mechanisms underlying the disease and the cellular functions of ABL1. From this perspective, the present study focuses on the recombinant expression, purification, and crystallization trials of the recombinant human ABL1 kinase domain for further structural analysis via X-ray crystallography.

Chapter 2

MATERIALS AND METHODS

2.1. Materials and Equipment

2.1.1. Stock solutions and LB medium

LB medium (Table 2.1) and stock solutions of antibiotics and 0.4 M IPTG (Table 2.2) were prepared to be used in transformation and protein expression experiments.

Table 2.1: LB Medium

Reagent	Amount (g/L)
Tryptone	10
NaCl	10
Yeast extract	5
Total	25

Table 2.2: Antibiotics and 0.4 M IPTG Stock Solutions

Reagent	Amount (mg/ml)
Kanamycin	50
Chloramphenicol	35
IPTG	95.324

2.1.2. Buffers

For small-scale expression check and protein purification, lysis buffers (Table 2.3), Ni-NTA affinity chromotogrpahy purification buffers (Table 2.4), and SEC buffer (Table 2.5) were prepared.

Table 2.3: Lysis Buffers

Regular Lysis Buffer		
Reagent	Final concentration	Amount
NaCl	500 mM	29.22 g
Tris	50 mM	6.06 g
Imidazole	20 mM	1.362 g
Glycerol	5% (v/v)	50 ml
TritonX-100	0.1% (v/v)	5 ml
ddH2O		Upto 1 L
Total		1 L
High Salt Lysis Buffer		
Reagent	Final concentration	Amount
NaCl	1 M	58.44 g
Tris	50 mM	6.06 g
Imidazole	20 mM	1.362 g
Glycerol	5% (v/v)	50 ml
TritonX-100	0.1% (v/v)	5 ml
ddH2O		Upto 1 L
Total		1 L
8 M Urea Lysis Buffer		
Reagent	Final concentration	Amount
NaCl	500 mM	29.22 g
Tris	50 mM	6.06 g
Imidazole	20 mM	1.362 g
Glycerol	5% (v/v)	50 ml
TritonX-100	0.1% (v/v)	5 ml
Urea	8 M	480.48 g
ddH2O		Upto 1 L
Total		1 L
%0.5 Sarkosyl Lysis Buffer		
Reagent	Final concentration	Amount
NaCl	500 mM	29.22g

Tris	50 mM	6.06g
Imidazole	20 mM	1.362 g
Glycerol	5% (v/v)	50 ml
TritonX-100	0.1% (v/v)	5 ml
Sarkosyl	0.5% (m/v)	5 g
ddH2O		Upto 1 L
Total		1 L

Table 2.4: Ni-NTA Chromotgraphy Purification Buffers

His A Buffer		
Reagent	Final concentration	Amount
NaCl	200 mM	11.688 g
Tris	20 mM	6.06 g
Imidazole	20 mM	1.362 g
ddH2O		upto1 L
Total		1 L
Wash Buffer		
Reagent	Final concentration	Amount
NaCl	200 mM	11.688 g
Tris	20 mM	6.06 g
ddH2O		upto1 L
Total		1 L
His B Buffer		
Reagent	Final concentration	Amount
NaCl	200 mM	11.688 g
Tris	20 mM	6.06 g
Imidazole	250 mM	17.019 g
ddH2O		upto1 L
Total		1 L

Table 2.5: SEC Buffer

Reagent	Final concentration	Amount
NaCl	200 mM	11.688 g

Tris	20 mM	6.06 g
ddH2O		upto1 L
Total		1 L

2.2. Bacterial Transformation

The human ABL1 kinase domain gene was cloned into pET-28a(+) bacterial expression vector containing an N-terminal 6x-Histidine tag (Figure 2.1) and SUMO-tag with ULP1 protease cut site. The amino acid sequences of the ABL1 kinase domain construct with the N-terminus SUMO-tag shown in bold is given below.

Human ABL1 Kinase Domain:

MSDSEVNQEAKPEVKPEVKPETHINLKVSDGSSEIFFKIKKTTPLRRLM EAFAKRQGKEMDSLRFLYDGIRIQADQTPEDLDMEDNDIIEAHREQIGGVS PNYDKWEMERTDITMKHKGGGGQYGEVYEGVWKKYSLTVAVKTLKEDTME VEEFLKEAAVMKEIKHPNLVQLLGVCTREPPFYIITEFMTYGNLLDYLRECNRQ EVNAVVLLYMATQISSAMEYLEKKNFIHRDLAARNCLVGENHLVKVADFGLS RLMTGDTYTAHAGAKFPIKWTAPESLAYNKFSIKSDVWAFGVLLWEIATYGMS PYPGIDLSQVYELLEKDYRMERPEGCPEKVYELMRACWQWNPSDRPSFAEIHQ AFETMFQES*

The cloned pET-28a(+) vector was transformed into an *Escherichia coli* BL21 Rosetta2^{TM} competent cell. The plasmid vector and the competent cell were thawed on ice for 20 minutes. Then, 2 µl of plasmid was mixed with 50 µl of the competent cells in a sterile Eppendorf tube and mixed gently by pipetting. The plasmid-competent cell mixture was incubated on ice for 20 minutes. Following the incubation, the competent cells were treated with heat shock at 42°C for 45 seconds. Afterward, the plasmid-competent cell mixture was incubated on ice for 2 minutes. Then, 500 µl of LB medium without antibiotics was added to the plasmid-competent cell mixture, and the cells were incubated at 37°C for 90 minutes.

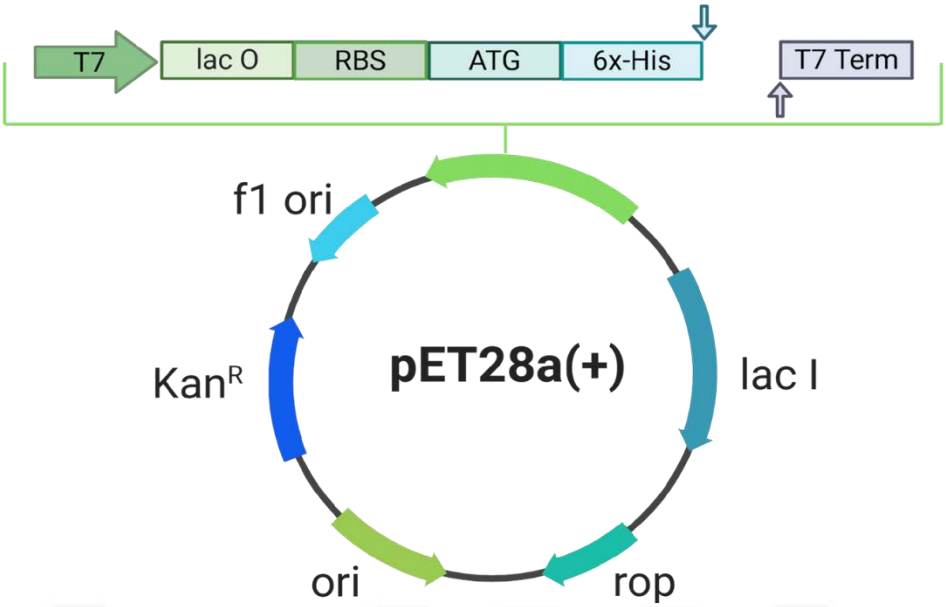

Figure 2.1: The plasmid map of the bacterial expression vector pET-28a(+).

After the incubation, the tube was centrifuged at 1500 rpm for 2 minutes and the supernatant was discarded. The pellet was gently resuspended in the remaining supernatant by pipetting. 50 µl of the cells were inoculated onto the LB agar plate with 50 µg/ml Kanamycin and 35 µg/ml Chloramphenicol, and spread on the agar plate by sterile glass beads. Then, the plate was incubated overnight at 37°C. Following the incubation, the colonies grown on the agar plate were inoculated into the LB medium with 50 µg/ml Kanamycin and 35 µg/ml Chloramphenicol using a micropipette and the cell culture was incubated at 37°C at 110 rpm overnight.

After the incubation, 750 µl cell culture was mixed with 750 µl sterilized 80% glycerol into a cryotube and mixed by vortexing. The glycerol stocks were stored at -80°C.

2.3. Mini-Scale Protein Expression

For the mini-scale protein expression assay, 5 ml of LB (50 g/L) medium (refer Table 2.1) was prepared and autoclaved at 121°C for 20 minutes. 50 µg/ml Kanamycin and 35 µg/ml Chloramphenicol antibiotics were added into sterile LB medium and ABL1 glycerol stock was inoculated into prepared LB media. Next, cell culture was incubated at 37°C at 110 rpm overnight. After overnight incubation, 1 ml “before induction” sample was taken and centrifuged at 6000 rpm for 5 minutes at 4°C. The supernatant was

discarded, and the pellet was stored at -45°C. Protein expression in the remaining cell culture was induced with 0.4 mM IPTG (isopropyl β-D-1-thiogalactopyranoside) and cell culture was incubated at 18°C at 110 rpm overnight. Following the incubation, the cells were harvested by centrifugation at 6000 rpm for 5 minutes at 4°C.

The pellet was resuspended in a 750 µl regular lysis buffer (refer Table 2.3) and sonicated until completely resuspended. Next, the cell lysate was centrifuged at 10000 rpm for 10 minutes at 4°C. The supernatant was transferred into a clean tube and mixed with 40 µl Ni-NTA beads and incubated at 4°C for 4 hours. After incubation with the beads, the sample was centrifuged at 1000 rpm for 1 minute at 4°C. Then, the supernatant was carefully discarded. Next, 750 µl HisA buffer (refer Table 2.4) was added into the tube and incubated on ice for 30 minutes. Following the incubation, the sample was centrifuged at 1000 rpm for 1 minute at 4°C, and the supernatant was discarded. 40 µl HisB buffer(refer Table 2.4) was added into the tube and incubated on ice for 3 minutes. Following the incubation, the sample was centrifuged at 1000 rpm for 1 minute at 4°C and supernatant was taken into a new clean tube.

40 µl of samples were taken from each step during the assay—the before-induction, after-induction, pellet, supernatant and pull-down—and the samples were mixed with 10 µl of loading dye. Then, SDS-PAGE electrophoresis was performed to determine protein expression levels in these samples.

2.4. Optimization of Induction Conditions

For each tested condition 5 ml of LB (50 g/L) medium (refer Table 2.1) was prepared and autoclaved at 121°C for 20 minutes. 50 µg/ml Kanamycin and 35 µg/ml Chloramphenicol antibiotics were added into sterile LB medium and ABL1 glycerol stock was inoculated into prepared LB media. Cell cultures were incubated at 37°C at 110 rpm overnight.

2.4.1. Optimization of Induction Temperature

After overnight incubation, protein expression in the remaining cell culture was induced with 0.4 mM IPTG and cell cultures were incubated at 18°C and 20 °C at 110 rpm overnight. Pellets were resuspended in a 750 µl regular lysis buffer (refer Table 2.3) and sonicated until completely resuspended. Next, the cell lysates were centrifuged at

10000 rpm for 10 minutes at 4°C. The supernatants were transferred into clean tubes and mixed with 40 µl Ni-NTA beads and incubated at 4°C for 4 hours. After incubation with the beads, the samples were centrifuged at 1000 rpm for 1 minute at 4°C. Then, the supernatants were carefully discarded. Next, 750 µl HisA buffer (refer Table 2.4) was added into tubes and incubated on ice for 30 minutes. Following the incubation, the samples were centrifuged at 1000 rpm for 1 minute at 4°C, and the supernatants were discarded. 40 µl HisB buffer (refer Table 2.4) was added into tubes and incubated on ice for 3 minutes. Following the incubation, the samples were centrifuged at 1000 rpm for 1 minute at 4°C and supernatants were taken into a new clean tube.

40 µl of samples were taken from each step during the assay—after-induction, pellet, supernatant and pull-down—and the samples were mixed with 10 µl of loading dye. Then, SDS-PAGE electrophoresis was performed to determine protein expression levels in these samples.

2.4.2. Optimization of IPTG Concentration

After overnight incubation, the protein expression was induced with 0.2 mM and 0.4 mM IPTG and cell cultures were incubated at 18°C at 110 rpm overnight. Pellets were resuspended in a 750 µl regular lysis buffer (refer Table 2.3) and sonicated until completely resuspended. Next, the cell lysates were centrifuged at 10000 rpm for 10 minutes at 4°C. The supernatants were transferred into clean tubes and mixed with 40 µl Ni-NTA beads and incubated at 4°C for 4 hours. After incubation with the beads, the samples were centrifuged at 1000 rpm for 1 minute at 4°C. Then, the supernatants were carefully discarded. Next, 750 µl HisA buffer (refer Table 2.4) was added into tubes and incubated on ice for 30 minutes. Following the incubation, the samples were centrifuged at 1000 rpm for 1 minute at 4°C, and the supernatants were discarded. 40 µl HisB buffer (refer Table 2.4) was added into tubes and incubated on ice for 3 minutes. Following the incubation, the samples were centrifuged at 1000 rpm for 1 minute at 4°C and supernatants were taken into a new clean tube.

40 µl of samples were taken from each step during the assay—after-induction, pellet, supernatant and pull-down—and the samples were mixed with 10 µl of loading dye. Then, SDS-PAGE electrophoresis was performed to determine protein expression levels in these samples.

2.4.3. Optimization of Induction Duration

10 ml of LB (50 g/L) medium (refer Table 2.1) was prepared and autoclaved at 121°C for 20 minutes. 50 µg/ml Kanamycin and 35 µg/ml Chloramphenicol antibiotics were added into sterile LB medium and ABL1 glycerol stock was inoculated into prepared LB media. Next, cell cultures were incubated at 37°C at 110 rpm overnight. After overnight incubation, 1 ml "before induction" sample was taken and centrifuged at 6000 rpm for 5 minutes at 4°C. The supernatant was discarded, and the pellet was stored at -45°C. Protein expression in the remaining cell culture was induced with 0.4 mM IPTG and cell cultures were incubated at 18°C at 110 rpm overnight. After IPTG induction, 1 mL of culture was collected at 1, 2, 3, 4, 5, 6, and 7 hours, as well as after overnight incubation, and centrifuged at 6000 rpm for 5 minutes at 4°C.

Each pellet was resuspended in a 750 µl regular lysis buffer (refer Table 2.3) and sonicated until completely resuspended. 40 µl of samples were taken from each sample and the samples were mixed with 10 µl of loading dye. Then, SDS-PAGE electrophoresis was performed to determine protein expression levels in these samples.

2.5. Optimization of Lysis Buffer Composition

50 ml of LB (50 g/L) medium (refer Table 2.1) was prepared and autoclaved at 121°C for 20 minutes. 50 µg/ml Kanamycin and 35 µg/ml Chloramphenicol antibiotics were added into sterile LB medium and ABL1 glycerol stock was inoculated into prepared LB media. Next, cell cultures were incubated at 37°C at 110 rpm overnight. After overnight incubation, 1 ml "before induction" sample was taken and centrifuged at 6000 rpm for 5 minutes at 4°C. The supernatant was discarded, and the pellet was stored at -45°C. Protein expression in the remaining cell culture was induced with 0.4 mM IPTG and cell cultures were incubated at 18°C at 110 rpm overnight. Following the incubation, the cell culture was divided into 10 Eppendorf tubes and harvested by centrifugation at 6000 rpm for 5 minutes at 4°C. The pellets were stored at -45°C.

2.5.1. Optimization of Lysis Buffer pH

Each pellet was resuspended in 750 µl regular lysis buffers (refer Table 2.1) with varying pHs- pH 4.5, pH 7.5, pH 9.0- and sonicated until completely resuspended. Next,

the cell lysates were centrifuged at 10000 rpm for 10 minutes at 4°C. The supernatants were transferred into a clean tube and mixed with 40 µl Ni-NTA beads and incubated at 4°C for 4 hours. After incubation with the beads, the samples were centrifuged at 1000 rpm for 1 minute at 4°C. Then, the supernatants were carefully discarded. Next, 750 µl His A buffer (refer Table 2.4) with varying pHs- pH 4.5, pH 7.5, pH 9.0- was added into tubes and incubated on ice for 30 minutes. Following the incubation, samples were centrifuged at 1000 rpm for 1 minute at 4°C, and supernatants were discarded. 40 µl His B buffer (refer Table 2.4) with varying pHs- pH 4.5, pH 7.5, pH 9.0- was added into tubes and incubated on ice for 3 minutes. Following the incubation, samples were centrifuged at 1000 rpm for 1 minute at 4°C and supernatants were taken into new clean tubes.

40 µl of samples were taken from each step of each tested condition during the assay—the before-induction, after-induction, pellet, supernatant and pull-down—and the samples were mixed with 10 µl of loading dye. Then, SDS-PAGE electrophoresis was performed to determine protein expression levels in these samples.

2.5.2. Optimization of Lysis Buffer Salt Concentration

Each pellet was resuspended in 750 µl lysis buffers (refer Table 2.3) with varying NaCl concentrations- 500 mM and 1 M NaCl- and sonicated until completely resuspended. Next, the cell lysates were centrifuged at 10000 rpm for 10 minutes at 4°C. The supernatants were transferred into a clean tube and mixed with 40 µl Ni-NTA beads and incubated at 4°C for 4 hours. After incubation with the beads, the samples were centrifuged at 1000 rpm for 1 minute at 4°C. Then, the supernatants were carefully discarded. Next, 750 µl His A buffer (refer Table 2.4) was added into tubes and incubated on ice for 30 minutes. Following the incubation, samples were centrifuged at 1000 rpm for 1 minute at 4°C, and supernatants were discarded. 40 µl His B buffer (refer Table 2.4) was added into tubes and incubated on ice for 3 minutes. Following the incubation, samples were centrifuged at 1000 rpm for 1 minute at 4°C and supernatants were taken into new clean tubes.

40 µl of samples were taken from each step of each tested condition during the assay—the before-induction, after-induction, pellet, supernatant and pull-down—and the samples were mixed with 10 µl of loading dye. Then, SDS-PAGE electrophoresis was performed to determine protein expression levels in these samples.

2.5.3. Detergent Screening

Each pellet was resuspended in 750 µl lysis buffers (refer Table 2.3) with varying detergent compositions- %0.5 sarkosyl and 8 M urea- and sonicated until completely resuspended. Next, the cell lysates were centrifuged at 10000 rpm for 10 minutes at 4°C. The supernatants were transferred into a clean tube and mixed with 40 µl Ni-NTA beads and incubated at 4°C for 4 hours. After incubation with the beads, the samples were centrifuged at 1000 rpm for 1 minute at 4°C. Then, the supernatants were carefully discarded. Next, 750 µl HisA buffer (refer Table 2.4) was added into tubes and incubated on ice for 30 minutes. Following the incubation, samples were centrifuged at 1000 rpm for 1 minute at 4°C, and supernatants were discarded. 40 µl HisB buffer (refer Table 2.4) was added into tubes and incubated on ice for 3 minutes. Following the incubation, samples were centrifuged at 1000 rpm for 1 minute at 4°C and supernatants were taken into new clean tubes.

40 µl of samples were taken from each step of each tested condition during the assay—the before-induction, after-induction, pellet, supernatant and pull-down—and the samples were mixed with 10 µl of loading dye. Then, SDS-PAGE electrophoresis was performed to determine protein expression levels in these samples.

2.5.4. Optimization of Urea Concentration

Each pellet was resuspended in 750 µl lysis buffers containing varying concentrations of urea 2M, 4M, 6M and 8M and sonicated until completely resuspended. By using the formula of C1V1 = C2V2, buffers containing 2 M, 4 M, and 6 M urea were prepared by diluting 8 M and 0 M urea, regular lysis buffer, (refer Table 2.4). Next, the cell lysates were centrifuged at 10000 rpm for 10 minutes at 4°C. The supernatants were transferred into a clean tube and mixed with 40 µl Ni-NTA beads and incubated at 4°C for 4 hours. After incubation with the beads, the samples were centrifuged at 1000 rpm for 1 minute at 4°C. Then, the supernatants were carefully discarded. Next, 750 µl HisA buffer (refer Table 2.4) was added into tubes and incubated on ice for 30 minutes. Following the incubation, samples were centrifuged at 1000 rpm for 1 minute at 4°C, and supernatants were discarded. 40 µl HisB buffer (refer Table 2.4) was added into tubes and incubated on ice for 3 minutes. Following the incubation, samples were centrifuged at 1000 rpm for 1 minute at 4°C and supernatants were taken into new clean tubes.

40 µl of samples were taken from each step of each tested condition during the assay—the before-induction, after-induction, pellet, supernatant and pull-down—and the samples were mixed with 10 µl of loading dye. Then, SDS-PAGE electrophoresis was performed to determine protein expression levels in these samples.

2.5.5. Optimizing Sarkosyl Concentration

Each pellet was resuspended in 750 µl lysis buffers containing varying concentrations of sarkosly %0.1, %0.5, %1 (refer Table 2.3) and sonicated until completely resuspended. Next, the cell lysates were centrifuged at 10000 rpm for 10 minutes at 4°C. The supernatants were transferred into a clean tube and mixed with 40 µl Ni-NTA beads and incubated at 4°C for 4 hours. After incubation with the beads, the samples were centrifuged at 1000 rpm for 1 minute at 4°C. Then, the supernatants were carefully discarded. Next, 750 µl HisA buffer (refer Table 2.4) was added into tubes and incubated on ice for 30 minutes. Following the incubation, samples were centrifuged at 1000 rpm for 1 minute at 4°C, and supernatants were discarded. 40 µl HisB buffer (refer Table 2.4) was added into tubes and incubated on ice for 3 minutes. Following the incubation, samples were centrifuged at 1000 rpm for 1 minute at 4°C and supernatants were taken into new clean tubes.

40 µl of samples were taken from each step of each tested condition during the assay—the before-induction, after-induction, pellet, supernatant and pull-down—and the samples were mixed with 10 µl of loading dye. Then, SDS-PAGE electrophoresis was performed to determine protein expression levels in these samples.

2.6. Large Scale Protein Expression and Purification

300 ml LB media (50 g/L) for starter culture and 6 x 1 L LB media (50 g/L) (refer Table 2.1) for large scale expression were prepared and autoclaved at 121°C for 20 minutes. 50 µg/ml Kanamycin and 35 µg/ml Chloramphenicol antibiotics were added into sterile LB medium and ABL1 glycerol stock was inoculated into prepared 50 ml LB media. Next, cell culture was incubated at 37°C at 110 rpm overnight.

After overnight incubation, 50 µg/ml Kanamycin and 35 µg/ml Chloramphenicol antibiotics were added into 1 L LB medium and starter culture was scaled-up to 1 L for large-scale expression. After scaling up, the OD600 of the cultures were measured using

a NanoDrop device every hour. When the OD600 reached approximately 0.8, the protein expression was induced by adding 0.4 mM IPTG. The culture was incubated overnight at 18°C at 110 rpm. Following the incubation, cells were harvested by centrifuging at 3500 rpm for 45 minutes, the supernatants were discarded and pellets were stored at -45°C.

2.6.1. Purification and Refolding Followed by Urea Solubilization

The pellet was placed on ice, 45 ml of lysis buffer containing 8 M urea (refer Table 2.3) was added to the falcon tube. The cells were sonicated for 1 second on and 1 second off for 30 seconds at 60% amplitude. Sonication was repeated until the pellets were dissolved completely. Next, the cell lysates were placed into ultracentrifuge tubes and balanced with the help of a weighing device. Cell lysates were ultracentrifuged with a Ti45 rotor in a Beckman Optima TM L-80XP Ultracentrifuge (Beckman, USA) at 25000 rpm for 1 hour 15 minutes at 4°C. Following centrifugation, the supernatant was discarded and the pellet was resuspended in 45 ml of ddH_2O and sonicated until the pellet was fully dissolved. Then, the sample was ultracentrifuged with a Ti45 rotor in a Beckman Optima TM L-80XP Ultracentrifuge (Beckman, USA) at 10000 rpm for 25 minutes at 4°C. This step was performed twice. After the second centrifugation, the pellet was dissolved within the 8 M urea containing lysis buffer (refer Table 2.3) and left overnight incubation on the stirrer at room temperature.

After the incubation, the sample was ultracentrifuged with a Ti45 rotor in a Beckman Optima TM L-80XP Ultracentrifuge (Beckman, USA) at 10000 rpm for 45 minutes at 4°C. The protein sample was purified using Ni-NTA affinity chromatography with a gravity-flow column. First, the column was washed with 3 column volumes of 1 M Imidazole. Then, it was equilibrated with 2 column volumes of HisA buffer containing 8 M Urea. Next, the filtered protein sample was loaded to the column while the flowthrough containing unbound proteins was collected. The column was again washed with column volume of gradient HisA buffers from 8 M urea to 0 M urea. Afterward, ABL1 was eluted from the Ni-NTA column by applying one column volume of His B buffer (refer Table 2.4). Then, the column was washed with 3 column volumes of 1 M Imidazole.

40 µl of samples were taken from each step of expression and purification and the samples were mixed with 10 µl of loading dye. SDS-PAGE was then performed to evaluate protein expression and purity at these stages. The eluted fractions showing the target protein band on the gel were concentrated using a 10 kDa MWCO concentrator.

2.6.2. Purification Followed by Sarkosyl Solubilization

The pellet was placed on ice, 45 ml of lysis buffer containing %0.5 sarkosyl (refer Table 2.3) was added to the falcon tube. The cells were sonicated for 1 second on and 1 second off for 30 seconds at 60% amplitude. Sonication was repeated until the pellets were dissolved completely. Next, the cell lysates were placed into ultracentrifuge tubes and balanced with the help of a weighing device. Cell lysates were ultracentrifuged with a Ti45 rotor in a Beckman Optima TM L-80XP Ultracentrifuge (Beckman, USA) at 25000 rpm for 1 hour 15 minutes at 4°C. Following centrifugation, the supernatant was dialyzed overnight at 4°C against 2 L of dialysis buffer using a 3 kDa molecular weight cut-off (MWCO) dialysis membrane.

After overnight dialysis, the protein sample was purified using Ni-NTA affinity chromatography with a gravity-flow column. First, the column was washed with 3 column volumes of 1 M Imidazole. Then, it was equilibrated with 2 column volumes of HisA buffer (refer Table 2.4). Next, the filtered protein sample was loaded to the column while the flowthrough containing unbound proteins was collected. The column was again washed with column volume of wash buffer (refer Table 2.4) to remove the unbound and nonspecifically bound proteins. Afterward, ABL1 was eluted from the Ni-NTA column by applying one column volume of His B buffer (refer Table 2.4). Then, the column was washed with 3 column volumes of 1 M Imidazole.

40 µl of samples were taken from each step of expression and purification and the samples were mixed with 10 µl of loading dye. SDS-PAGE was then performed to evaluate protein expression and purity at these stages. The eluted fractions showing the target protein band on the gel were concentrated using a 10 kDa MWCO concentrator.

The concentrated protein was flash-frozen in liquid nitrogen and stored at –80°C until further use.

2.7. 6X-His-SUMO-Tag Cleavage

The concentrated and purified ABL1 protein was subjected to 6xHis-SUMO tag cleavage using ULP1 protease under varying enzyme-to-protein ratios and incubation temperatures. For each condition, 100 µL of purified ABL1 was transferred into a clean Eppendorf tube, and ULP1 was added at ratios of 1:1000, 5:1000, and 1:100

(ULP1:protein). The tubes were then incubated at 4 °C, room temperature, and 37 °C. After the initiation of the cleavage reaction, samples were collected at 1, 2, and 4 hours, as well as after overnight incubation. 40 µl of samples were mixed with 10 µl of loading dye. Then, SDS-PAGE electrophoresis was performed to evaluate the efficiency of 6X-His–SUMO tag cleavage under tested conditions.

2.8. Reverse Chromatography

After the optimization of the enzymatic conditions for 6X-His-SUMO-Tag was cleavage in mini-scale, the cleavage of N-terminal 6X-His-SUMO-Tag was performed in large-scale followed by Reverse Chromatography. The cleavage was performed with 1:100 ULP1: protein ratio for overnight at 4°C. After the incubation, the separation of cleaved ABL1 from 6X-His-SUMO-Tag was performed by Reverse Chromatography using an AKTA-Go FPLC device with Ni-NTA column. First, the Ni-NTA column was washed 1 M Imidazole and then equilibrated with HisA buffer (refer Table 2.4) until the UV absorbance stabilized. After the equilibration of the column, the protein and ULP1 mixture was loaded into the column, and the flowthrough, which contains cleaved ABL1 proteins, was collected from the outlet valve. Afterward, the column was washed with His A buffer (refer Table 2.4). Then, for the elution of 6X-His-SUMO-Tag, HisB elution buffer (refer Table 2.4) was applied to the column.

40 µl of samples were taken from each step of purification and the samples were mixed with 10 µl of loading dye. SDS-PAGE was then performed to evaluate cleavage efficiency.

2.9. Size Exclusion Chromatography

Following the protein purification, size exclusion chromatography analysis was performed on an AKTA-Go FPLC device with the concentrated ABL1 sample. A SuperdexTM 200 (10/300 GL) column was used and equilibrated with SEC buffer (refer Table 2.5). Following the column equilibration, 2 mL of concentrated protein was manually injected using a 5 mL loop in the manual load mode of the AKTA-go system. Then, the system was set to inject mode for 10-minutes. Afterward, the system was returned to manual load mode. Following the sample injection, the SEC buffer was passed

through the column until UV was stabilized. All fractions were collected as 5 mL in 15 mL Falcon tubes.

40 µl of samples were taken from each fraction corresponding to UV peaks and were mixed with 10 µl of loading dye. SDS-PAGE was then performed to evaluate the protein expression. The protein fractions corresponding to the UV Peak were concentrated with a 10 kDa Amicon Ultra centrifugal filter tube.

2.10. Protein Crystallization and Crystal Screening

Crystallization of ABL-1 protein was performed using the microbatch under oil method in 72-well Terasaki crystallization plates. ABL-1 protein samples (0.83 µL) were mixed at a 1:1 ratio with 0.83 µL of each condition from approximately 3000 commercially available sparse matrix crystallization screening sets. 16.6 µL of paraffin oil was added to cover each well and the plates were stored at 4°C.In addition to apo-ABL1 crystallization trials, co-crystallization experiments were performed with the ABL-1 protein in the presence of the commercially available TKIs Imatinib and Dasatinib, as well as the novel hit compounds HT-A, Blg-AC, Dasa-Dtc, Bosu-A, MT-C, and HOA-1. Each inhibitor was individually added to protein aliquots until supersaturation was reached, and co-crystallization of the resulting protein–inhibitor mixtures was performed using the previously described method. The Terasaki plates were regularly controlled under the light microscope to monitor crystal formation. The observed crystals were analyzed at ambient temperature using Rigaku XtaLAB Synergy Flow X-ray Diffractometer “Turkish Light Source” (University of Health Sciences, Istanbul, Türkiye). Data collection at ambient temperature was conducted by setting the Oxford Cryosystems Cryostream 800 Plus to 300 K. The Terasaki plate was mounted on the XtalCheck-S plate reader (Gul et al., 2023), and multiple crystals were screened in the Terasaki plate to determine whether they were salt or protein crystals.

Chapter 3

RESULTS

3.1. Expression of ABL1

The transformation of the human ABL1 kinase domain into *E. coli* BL21 Rosetta2^{TM} cells was achieved by the heat-shock method. Following the transformation, the expression of recombinant ABL1 was tested on a mini-scale. In the SDS-PAGE analysis, a protein band around 42 kDa corresponding to the expected molecular weight of the human ABL1 kinase domain fused with SUMO-tag was detected (Figure 3.1) under the tested growth conditions. However, the majority of the expression was observed in the pellet rather than the supernatant. The presence of the recombinant ABL1 in the pellet indicates improper protein folding and its tendency for aggregation. The accumulation of the recombinant protein in the pellet suggests the need for further optimizations of growth conditions for soluble protein expression.

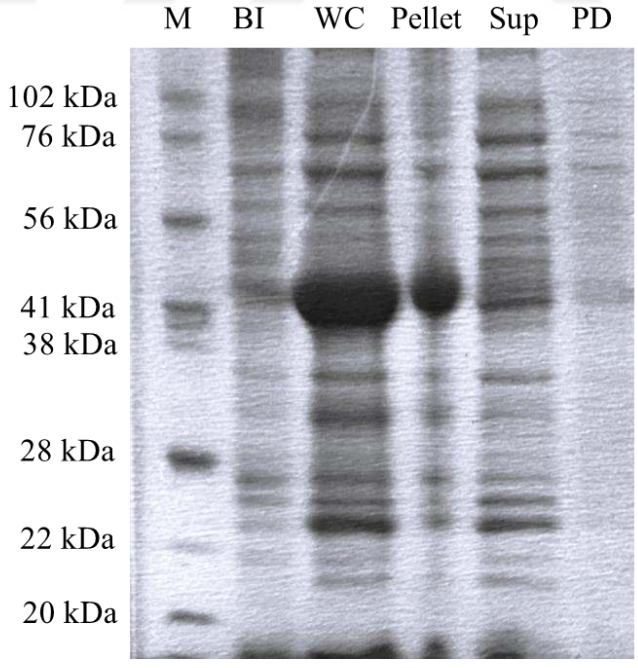

Figure 3.1: SDS-PAGE analysis of mini-scale expression of the ABL1 kinase domain. M: Marker, WC: Whole Cell Lysate, P: Pellet, Sup: Supernatant, PD: Pull down sample.

3.2. Optimization of Induction Conditions

To optimize the expression of recombinant ABL1, the protein expression was tested under different growth conditions, including varying induction temperatures, IPTG concentrations, and induction durations. First, the protein expression levels were tested under 18°C and 20 °C (Figure 3.2). Under both induction temperatures, the protein expression was observed around 42 kDa in the pellets as aggregates, suggesting that the soluble expression of protein was not affected by the temperature variations. When compared to 20°C, under 18°C induction, a thicker band indicating a higher level of protein expression was observed. In the following steps, the culture was induced at 18°C to achieve a higher level of protein expression.

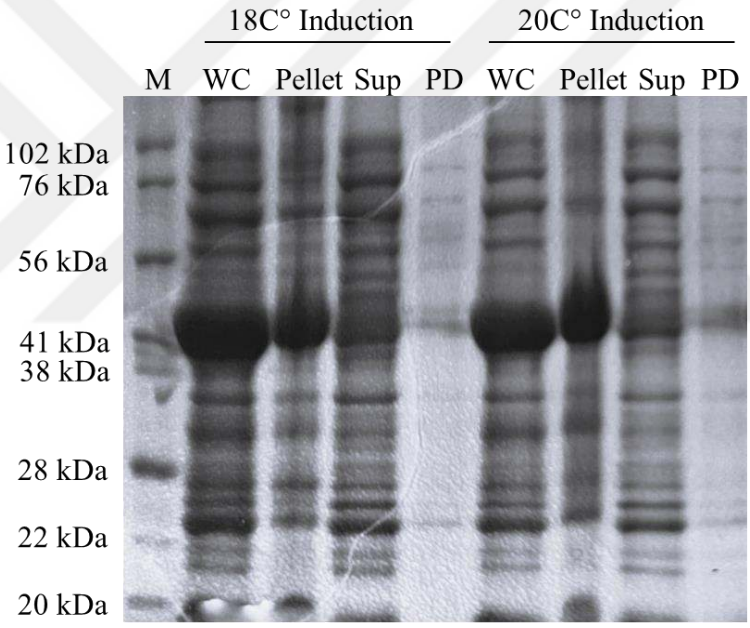

Figure 3.2: SDS-PAGE analysis of mini-scale expression of the ABL1 kinase domain at different temperatures (18°C, 20°C). M: Marker, WC: Whole Cell Lysate, Sup: Supernatant, PD: Pull down sample.

After optimizing the induction temperature, the protein expression levels were tested under induction with different concentrations of IPTG: 0.4 mM and 0.2 mM. Under the induction with both IPTG concentrations, the protein expression was observed in the pellets as aggregates rather than soluble fractions in the supernatant (Figure 3.3). According to the band thicknesses, the protein expression under the induction with 0.4 mM IPTG was observed to be higher than the expression under the induction with 0.2

mM IPTG. In the subsequent experiments, the cell culture was induced with 0.4 mM IPTG.

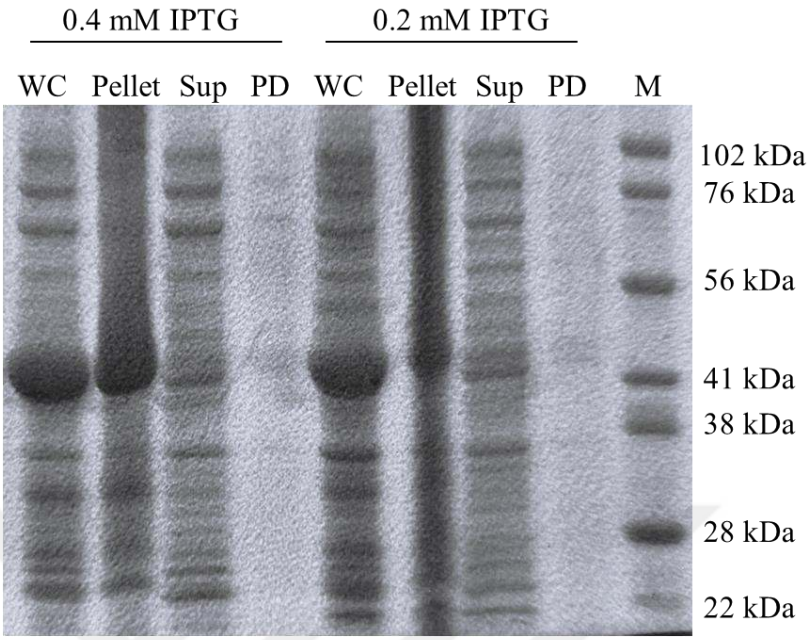

Figure 3.3: SDS-PAGE analysis of mini-scale expression of the ABL1 kinase domain under induction with different IPTG concentrations (0.2 mM, 0.4 mM). M: Marker, WC: Whole Cell Lysate, Sup: Supernatant, PD: Pull down sample.

In addition to the optimization of the induction temperature and IPTG concentration, the induction duration was optimized to enhance the protein expression. The protein expression was tested among different durations, including 1 to 7 hours and overnight incubation. In the SDS-PAGE analysis, a visible protein band around 42 kDa started to appear after 6 hours of incubation (Figure 3.4). According to the band thicknesses, the highest protein expression was detected in the overnight incubation.

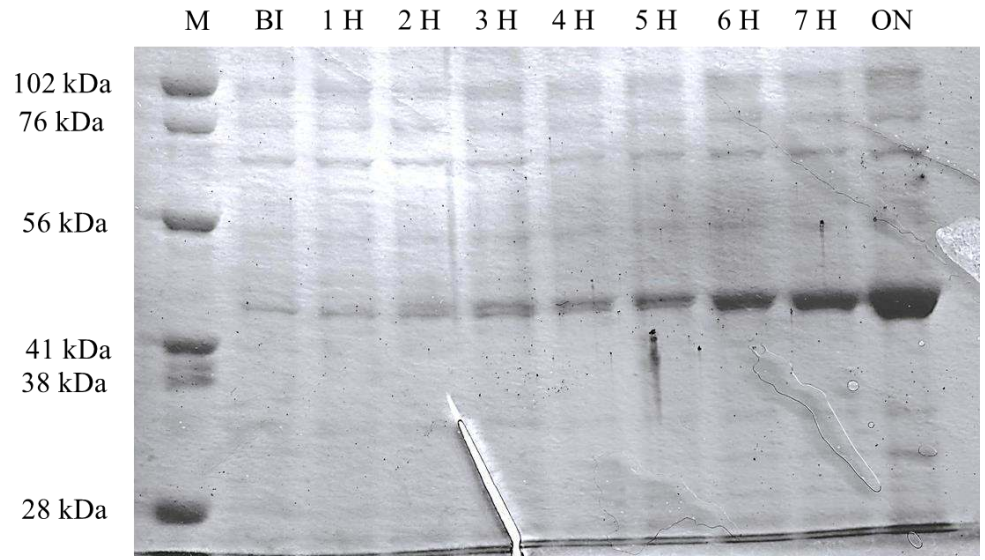

Figure 3.4: SDS-PAGE analysis of mini-scale expression of the ABL1 kinase domain under induction with different durations. M: Marker, BI: Before Induction, 1 H-ON: Whole cell lysates collected after 1 hour to ON incubation.

To achieve higher recombinant protein expression, the induction conditions, including the IPTG concentration, temperature, and duration, were optimized as 0.4 mM IPTG, 18°C, and overnight. Although the optimization of the culture conditions, the expression of recombinant ABL1 in the pellet rather than supernatant in the tested conditions demonstrated the need for further optimizations, especially in the buffer composition to solubilize the protein aggregates.

3.3. Soluble Expression of ABL1

After the optimization of the induction conditions to solubilize protein aggregates, lysis buffers with different compositions were used and the protein levels in the supernatant were analyzed by SDS-PAGE. First, the soluble protein levels were tested with lysis buffers varying pHs: pH 4.0, pH 7.5, and pH 9.0. However, in all tested pH conditions, the protein was observed in pellets rather than supernatant (Figure 3.5). Since the protein expression was not affected by the pH variations, the protein solubilization was tested with varying other components of the lysis buffer.

Following the pH, the soluble protein expression was tested under different salt concentrations: 500 mM and 1 M NaCl. Both in the low salt and high salt concentrations

the protein was observed in the pellet (Figure 3.6), which suggests the protein solubilization was not affected by the salt concentration.

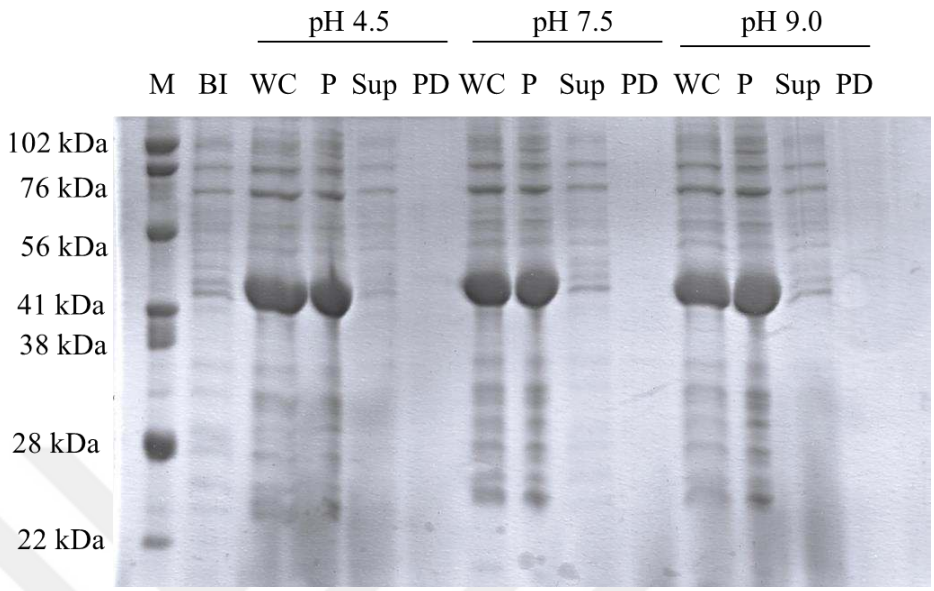

Figure 3.5: SDS-PAGE analysis of mini-scale ABL1 kinase domain expression subjected to lysis using buffers with different pH values (pH 4.0, pH 7.5, pH 9.0). M: Marker, WC: Whole Cell Lysate, P: Pellet, Sup: Supernatant, PD: Pull down sample.

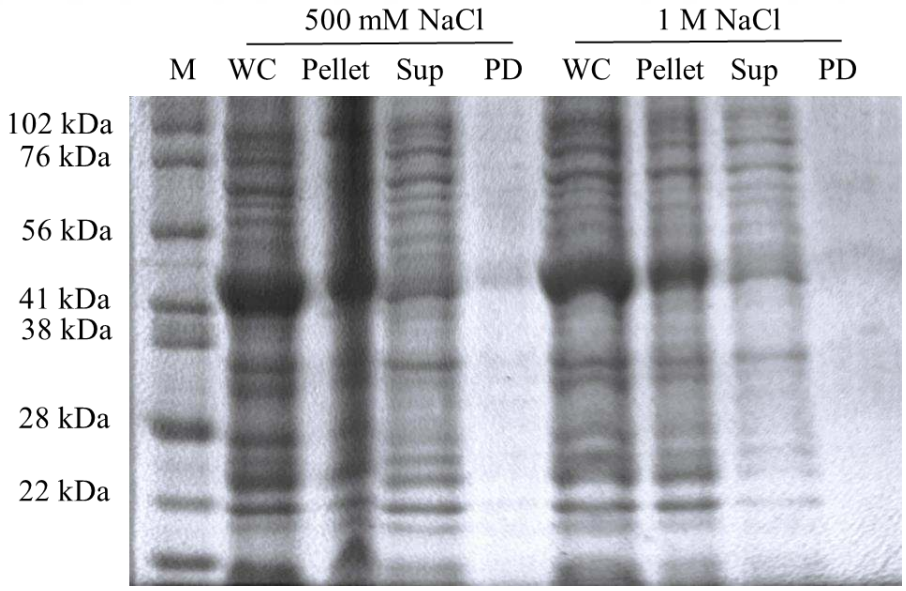

Figure 3.6: SDS-PAGE analysis of mini-scale ABL1 kinase domain expression subjected to lysis using buffers with different NaCl concentrations (0.5 mM, 1M). M: Marker, WC: Whole Cell Lysate, Sup: Supernatant, PD: Pull down sample.

Next, the soluble protein expression was tested under the detergent treatment. For this purpose 2 different detergents, urea and sarkosyl, were used. In the SDS-PAGE analysis, bands at 42 kDa were observed in the supernatant fractions under the treatment of both detergents (Figure 3.7). In addition to the soluble protein fractions that were observed in the supernatant, in the pull-down samples of both conditions, bands around 42 kDa, indicating the interaction of the soluble protein with Ni-NTA beads via its 6X-His tag, were observed. To optimize the soluble protein expression, in the next steps, the detergent concentrations in the lysis buffer were optimized.

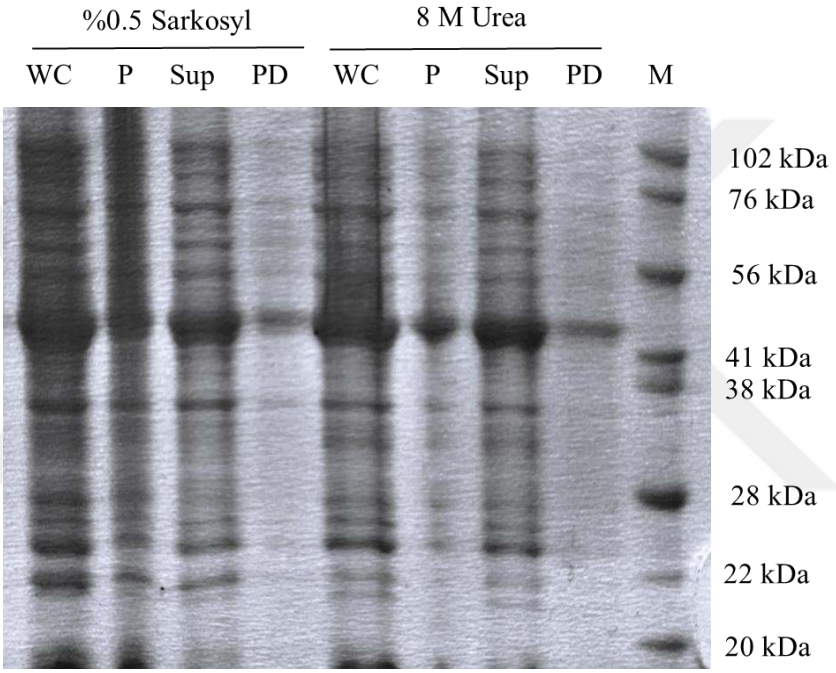

Figure 3.7: SDS-PAGE of mini-scale ABL1 kinase domain expression lysed with various detergent-containing buffers (8 M urea, %0.5 sarkosyl). M: Marker, WC: Whole Cell Lysate, P: Pellet, Sup: Supernatant, PD: Pull down sample.

To optimize the urea concentration for the highest soluble protein expression, the cell pellets were treated with varying concentrations of urea: 2 M, 4 M, 6 M, and 8 M, and the protein expressions were analyzed by SDS-PAGE. The soluble protein expression was increased with the increase of the urea concentrations, and the highest soluble protein expression was observed under the treatment with 8 M urea (Figure 3.8). Like the supernatant samples, for the pull-down samples, the band thickness increases with the increase of the urea concentration, and the thickest band, which indicates the highest level of protein interacting with Ni-NTA beads, was observed under the treatment of 8 M urea.

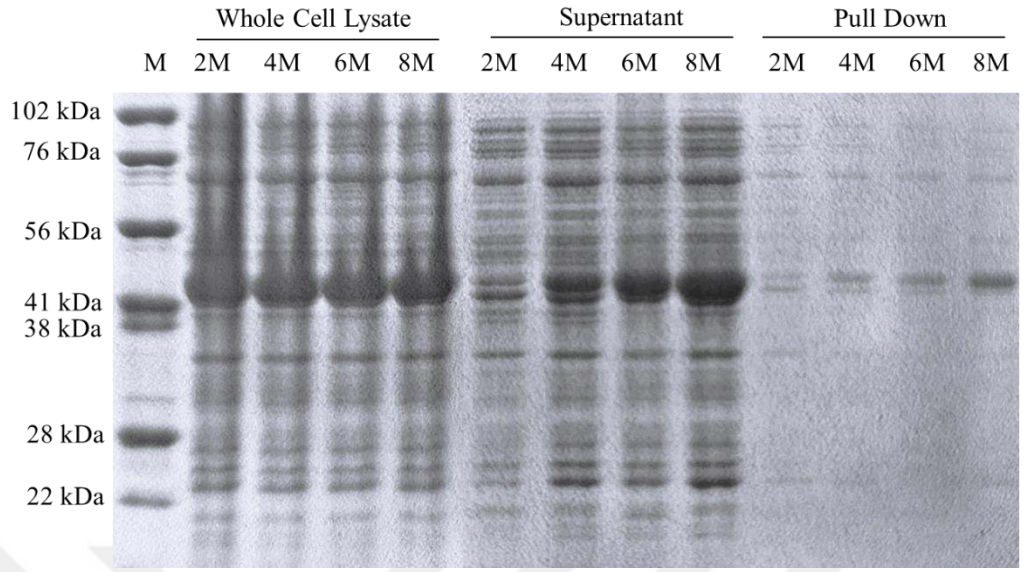

Figure 3.8: SDS-PAGE analysis of mini-scale ABL1 kinase domain expression following lysis with buffers containing varying concentrations of urea (0 M, 2 M, 4 M, 6 M, 8 M urea). M: Marker, WC: Whole Cell Lysate, Sup: Supernatant, PD: Pull down sample.

To optimize sarkosyl concentration in the lysis buffer for maximal soluble protein expression, the effects of various sarkosyl concentrations: %0.1, %0.5, and %1 on the protein solubility were tested. In the SDS-PAGE analysis, the soluble protein fractions in the supernatant were observed in all tested sarkosyl concentrations with varying band thickness and intensity (Figure 3.9). The increase in the band thickness, indicating a higher level of protein, was observed with the increase of sarkosyl concentration within the lysis buffer. For the pull-down samples, band thickness was observed as almost the same for the treatment with %0.5 and %1 sarkosyl. However, under treatment with %0.1 sarkosyl, a weak protein band which indicates a low level of protein interacting with Ni-NTA beads was observed when compared to pull-down samples of %0.5 and %1 sarkosyl.

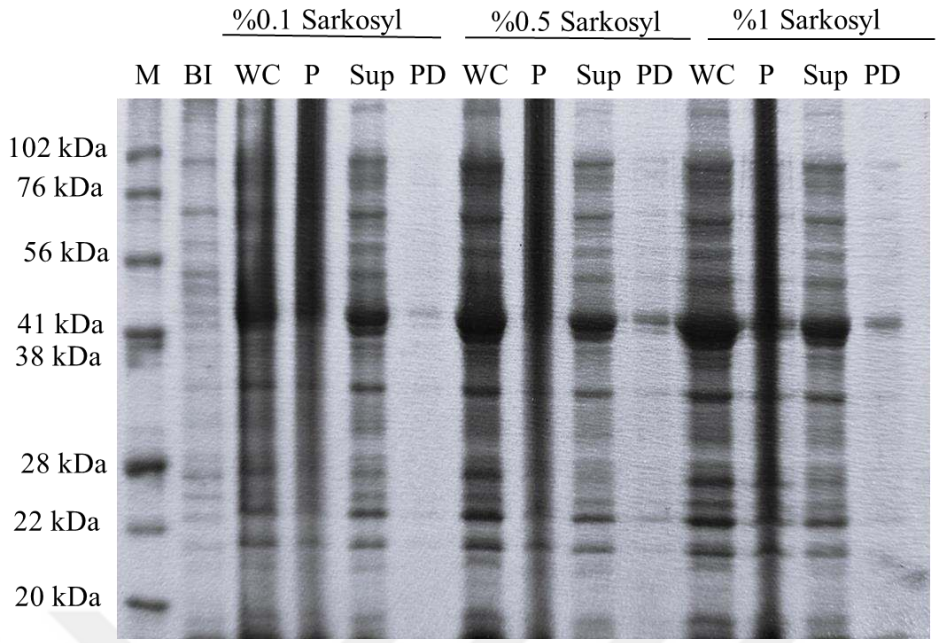

Figure 3.9: SDS-PAGE analysis of mini-scale ABL1 kinase domain expression following lysis with buffers containing varying concentrations of sarkosyl (%0.1, %0.5, %1). M: Marker, BI: Before Induction, WC: Whole Cell Lysate, P: Pellet, Sup: Supernatant, PD: Pull down sample.

In the subsequent steps, a lysis buffer containing %0.5 sarkosyl concentration was used as the lysis buffer. The main reason for the choice of %0.5 sarkosyl over %1 sarkosyl is keeping the detergent concentration at the minimum required to solubilize the protein. In this way, the elimination of the excess detergent in the environment was aimed.

3.4. Large-Scale Protein Expression & Purification

Following the optimization of the culture conditions and the lysis buffer composition in the mini-scale, the ABL1 was produced on a large scale in the optimized conditions, and the overexpressed recombinant protein was purified via Ni-NTA chromatography. For the large-scale protein expression and purification, both urea and sarkosyl-containing lysis buffers were used separately in different purification processes, and the efficiency of these methods over each other was tested.

3.4.1. Purification and Refolding Followed by Urea Solubilization

For urea-based solubilization and purification of ABL1, the overexpressed recombinant ABL1 was solubilized by 8 M urea, and the denatured protein sample was loaded on the gravity column. To enable folded protein, column refolding simultaneously to elution was performed by the gradient wash from 8 M urea to 0 M urea, followed by the elution with 250 mM Imidazole. In the SDS-PAGE analysis, bands at 42 kDa were observed in both flow-through, 8 M, and 7 M urea wash steps (Figure 3.10-a). Only, weak protein bands were observed in elution fractions E5 and E6 (Figure 3.10-b) with lower thickness and intensity compared with the bands in the flow-through and wash steps. These results indicate that the majority of the ABL1 did not interact with the column and flowed through. To enhance the efficiency of the protein purification, another protein-solubilizing detergent, sarkosyl, was used, and the purification efficiency was tested.

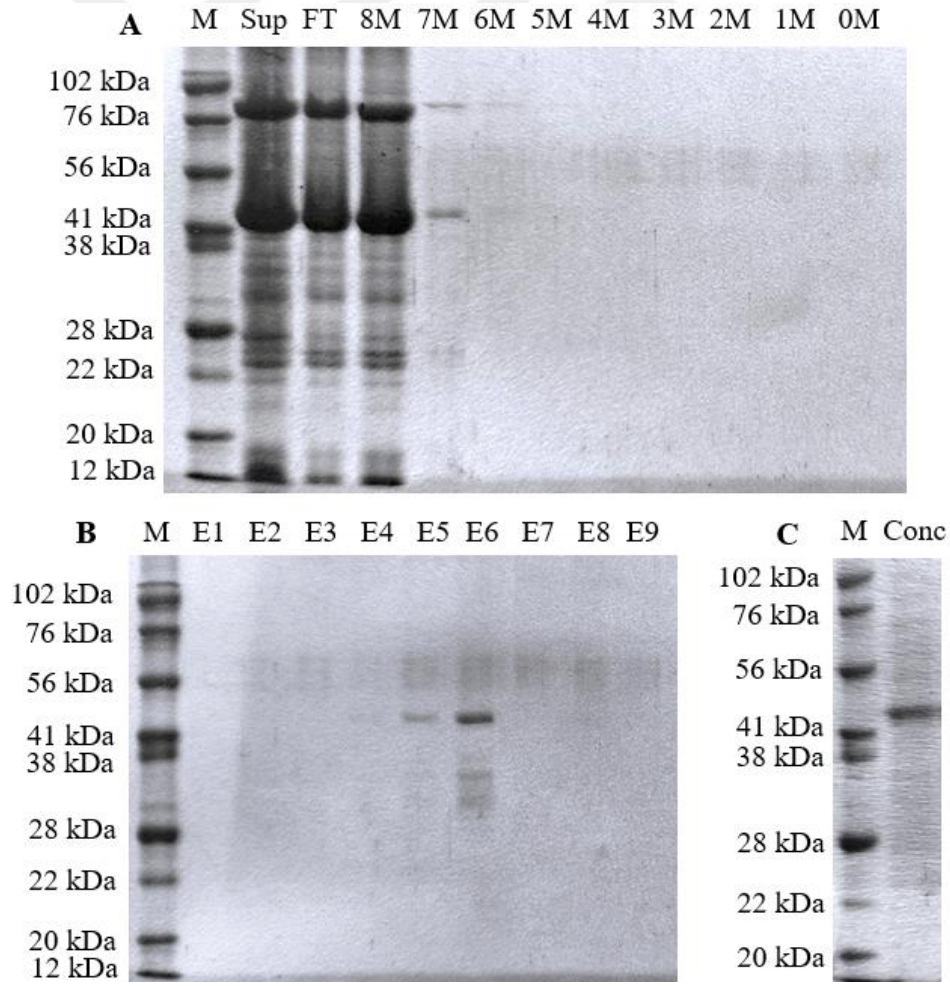

Figure 3.10: SDS-PAGE analysis of large-scale protein expression and purification of the ABL1 kinase domain followed by the urea solubilization. (a) Flowthrough and

wash steps. (a) Elution fractions. (c) Protein-containing elution fractions concentrated for further analysis.

3.4.2. Purification Followed by Sarkosyl Solubilization

After the urea refolding, the solubilization of the ABL1 via sarkosyl, followed by Ni-NTA chromatography using a gravity column, was performed. The supernatant sample, including overexpressed ABL1, was dialyzed overnight to decrease the sarkosyl concentration in the environment to enhance the protein purification. In the SDS-PAGE analysis, protein bands at 42 kDa corresponding to the expected molecular weight of ABL1 were observed in the elution fractions (Figure 3.11).

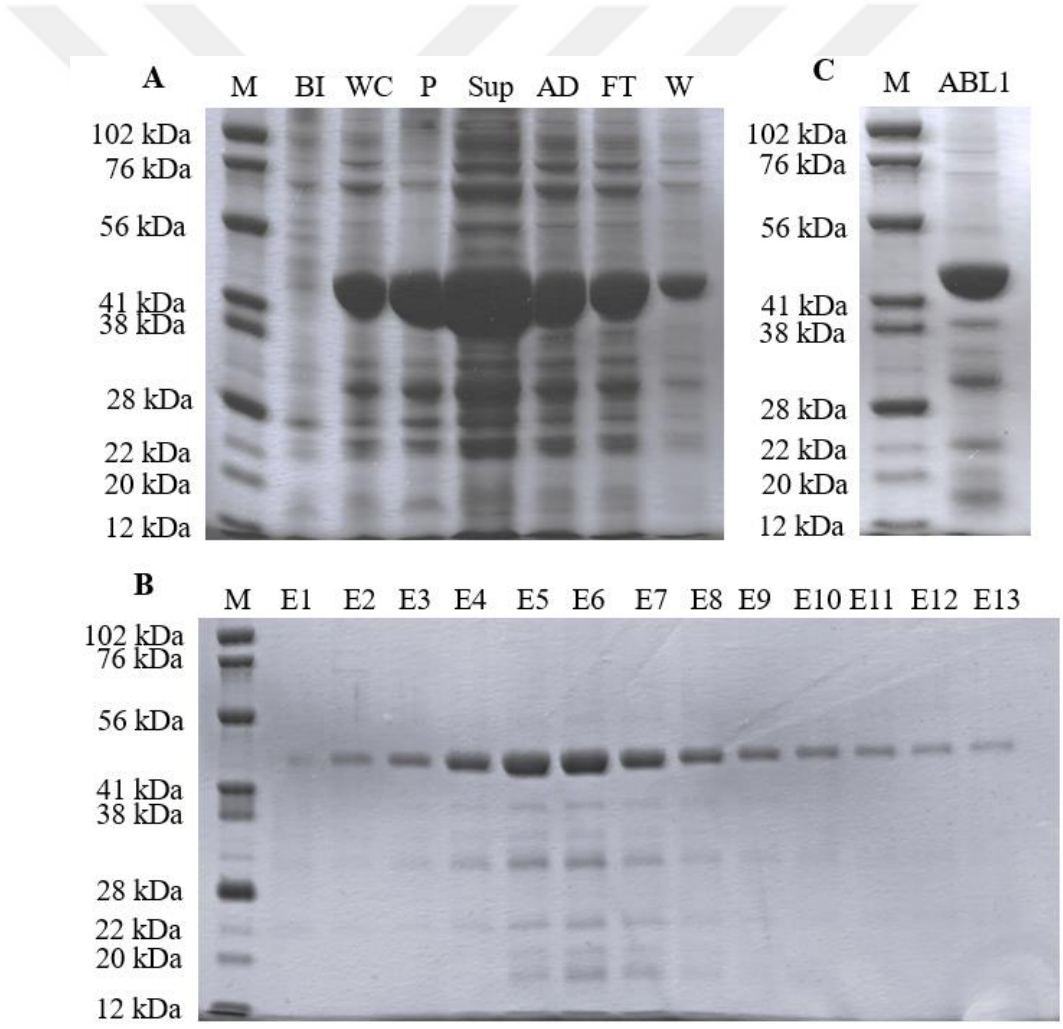

Figure 3.11: SDS-PAGE analysis of large-scale protein expression and purification of the ABL1 kinase domain followed by the sarkosyl solubilization. (a) Flowthrough and wash steps. (a) Elution fractions. (c) Protein-containing elution fractions concentrated for further analysis.

In addition to the protein bands in the elution fractions, in the flow-through and wash samples bands around 42 kDa indicating the unbound ABL1 were observed (Figure 3.11-a). The presence of a protein band at 42 kDa in the flow-through and wash samples demonstrates that some of the protein did not bind the column but instead flowed through. To increase the efficiency of the purification, the flow-through sample reloaded the column and the unbound ABL1 proteins were eluted. All elution fractions with protein bands at 42 kDa (Figure 3.11-b) were concentrated 20-fold with a 10 kDa MWCO filter (Figure 3.11-c). Due to its efficiency and simplicity over the urea method, in the large-scale expression and purification of the ABL1, the sarkosyl method was chosen and the concentrated protein after the sarkosyl purification was used in the following steps.

3.5. 6X-His-SUMO-Tag Cleavage

For the cleavage of 6X-His-SUMO-tag, the purified and concentrated ABL1 was treated with ULP1 protease. To optimize the cleavage efficiency, the enzymatic reaction was set up under different parameters, including varying enzyme to protein ratios, incubation temperature, and duration.

In all tested enzymatic conditions, both uncut ABL1 at 42 kDa, cut ABL1 without 6X-His-SUMO-tag at 28 kDa, and band at 13 kDa corresponding to the expected molecular weight of the SUMO-tag were observed in the SDS-PAGE analysis (Figure 3.12). The only exception is the enzymatic reaction that was set up with a 1:1000 enzyme: protein ratio that was incubated at 37°C (Figure 3.12-a). Even though the observed cut ABL1 at 28 kDa in almost all tested conditions, the cleavage efficiency varied among the tested conditions. A correlation between the cleavage efficiency of the 6X-His-SUMO tag and the ULP1 protease concentration was observed. The band thickness at 28 kDa corresponding to cut ABL1 without 6X-His-SUMO tag increases when the enzyme-to-protein ratio increases. Among the tested enzyme to protein ratios, the 1:100 ratio shows the highest cleavage efficiency (Figure 3.12-c).

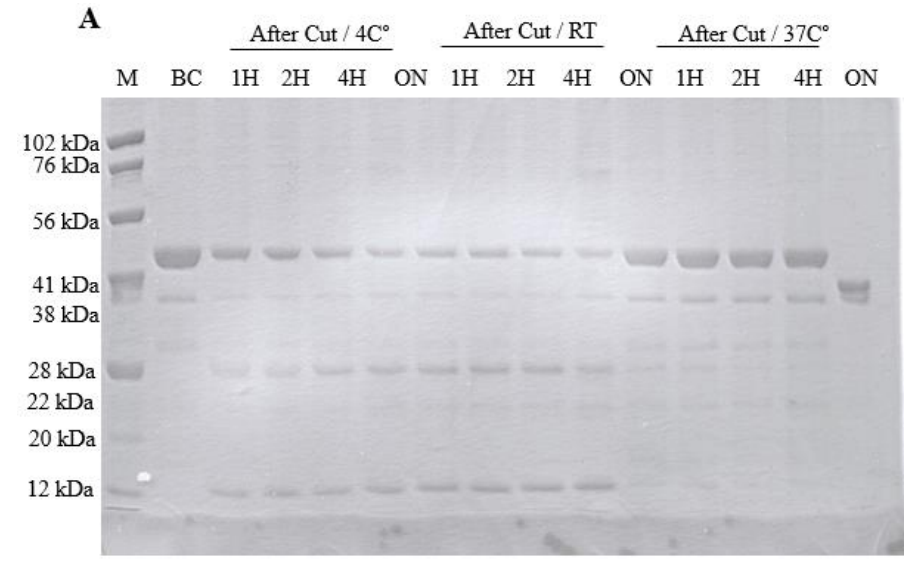

1:1000 (ULP1: Protein)

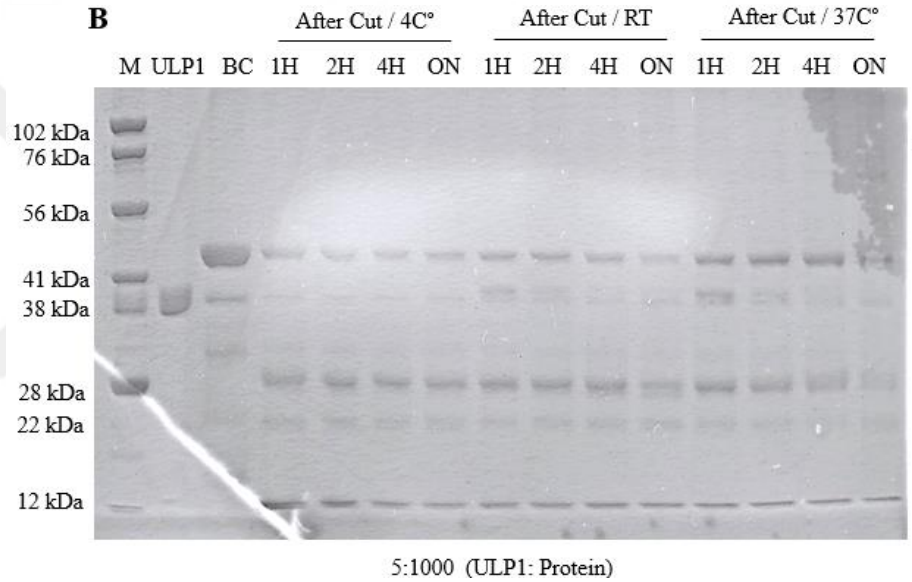

5:1000 (ULP1: Protein)

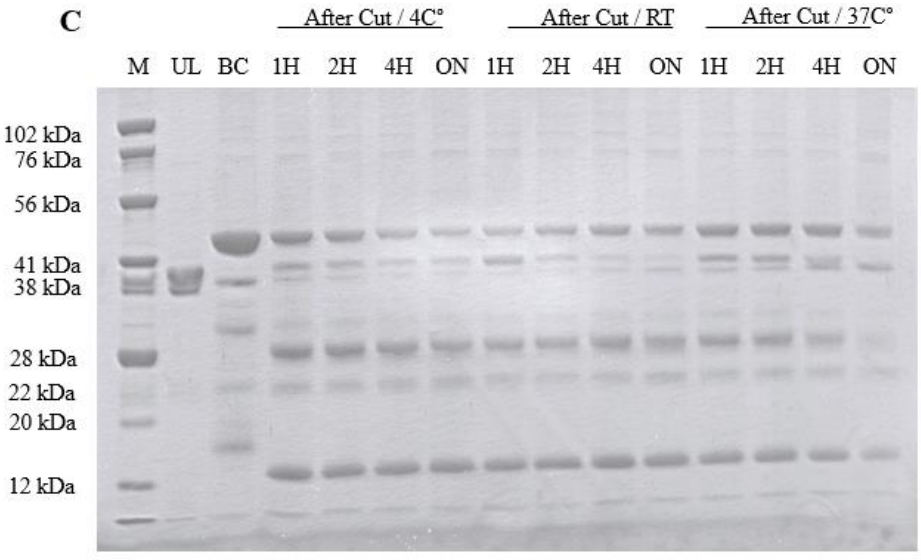

1:100 (ULP1: Protein)

Figure 3.12: SDS-PAGE analysis of 6X-His-SUMO tag cleavage by ULP1 under different enzymatic conditions. (a) 1:1000 enzyme to protein ratio. (b) 5:1000 enzyme to protein ratio. (c) 1:100 enzyme to protein ratio.

In addition to the optimization of the enzyme-to-protein ratio, the cleavage efficiency was tested for different incubation temperatures and durations. In the SDS-PAGE analysis, according to the band thickness and intensities, the highest cleavage efficiency with the thinnest bands at 42 kDa and thickest bands at 28 kDa was observed at 4C° incubation. In contrast, the lowest cleavage efficiency was observed under incubation at 37C°. As the last parameter for the enzymatic reaction, the induction duration was optimized. In the SDS-PAGE analysis, the protein band corresponding to cut ABL1 without 6X-His-SUMO tag at 28 kDa was observed in all durations, even for 1 hour incubation, for a 1:100 enzyme protein ratio at 4C°. However, the band thicknesses indicating the efficiency of the tag cleavage were changed among different durations. The highest cleavage efficiency was observed for 2-hour duration. The 6X-His-SUMO tag cleavage condition was optimized as a 1:100 enzyme to protein ratio, incubation at 4C° for 2 hours.

3.6. Reverse Chromatography

After optimizing the reaction conditions for the 6X-His-SUMO tag cleavage in mini-scale, the cleavage of the 6X-His-SUMO tag in large-scale, followed by reverse chromatography, was performed. The ULP1 protease was added to purified ABL1 in a 1:100 ratio and incubated at 4C° for 2 hours. In the SDS-PAGE analysis of the large-scale cleavage of 6X-His-SUMO tag and reverse chromatography, despite setting up the enzymatic reaction in optimized conditions, any cleavage of 6X-His-SUMO tag was not observed (Figure 3.13). Furthermore, similar to the result observed in the purification followed by the sarkosyl solubilization, the majority of the protein was also detected in the flow-through in the reverse chromatography, as supported by SDS-PAGE and chromatogram analysis.

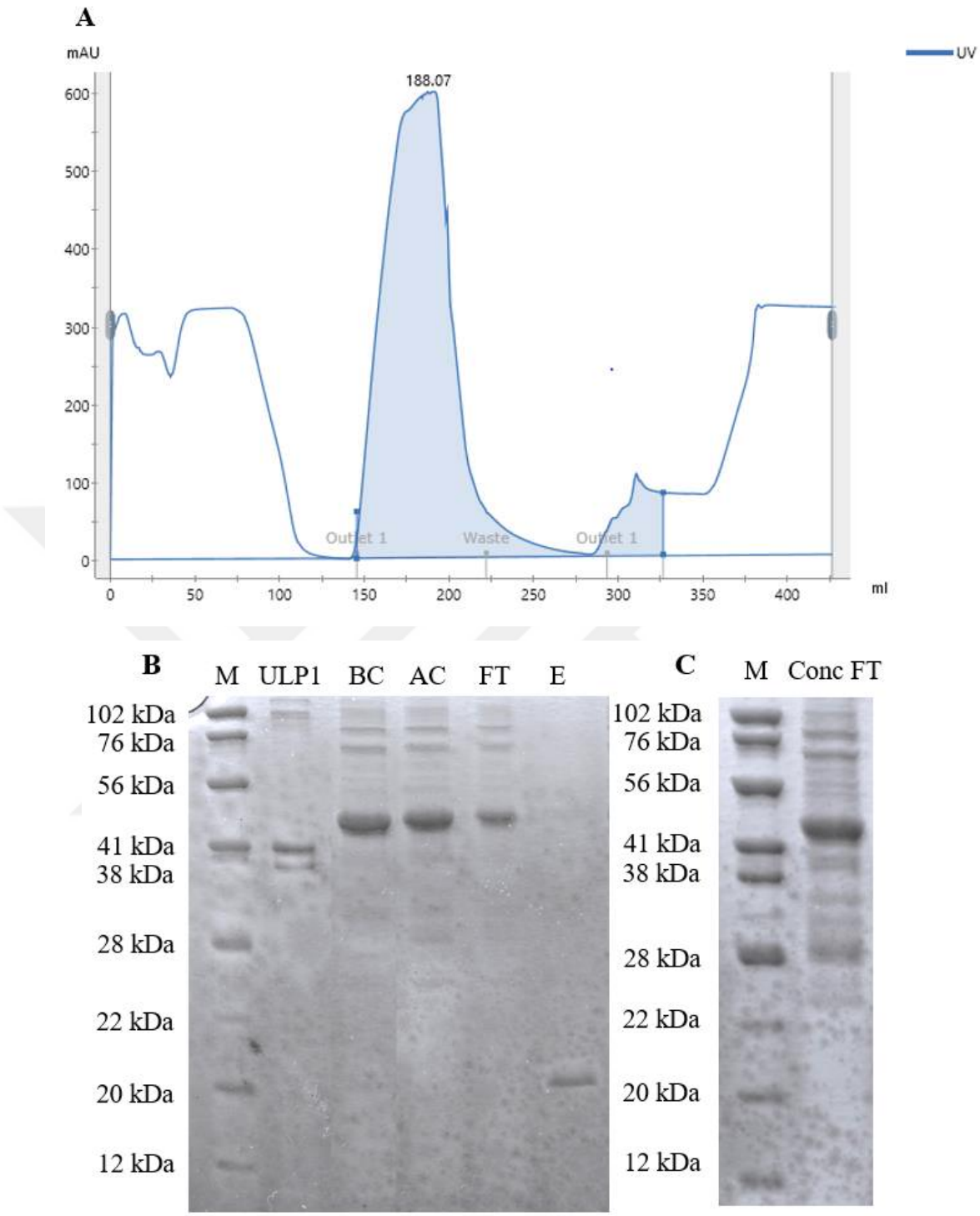

Figure 3.13: Reverse chromotography. (a) Reverse chromatography chromatogram. (b) SDS-PAGE results following reverse chromatography (c) Protein-containing elution fractions concentrated for further analysis.

3.7. Size Exclusion Chromotography

SEC analysis was performed to determine the oligomeric state of the expressed and purified ABL1. In the chromatogram, two major peaks with two minor peaks between them were observed (Figure 3.14-a). The fractions corresponding to the major and minor peaks were collected and analyzed by SDS-PAGE.

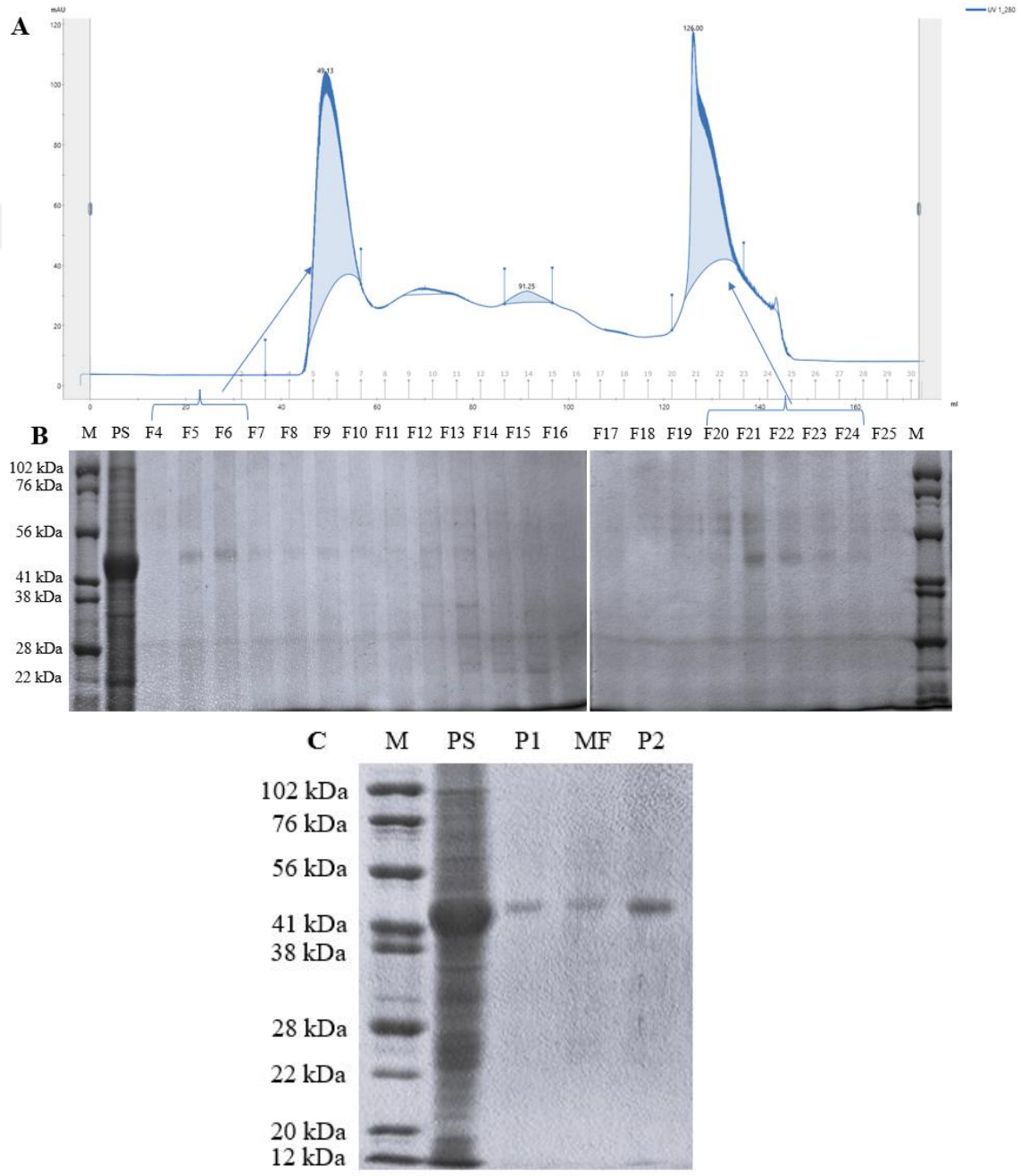

Figure 3.14: SEC analysis. (a) SEC chromatogram. (b) SDS-PAGE results following size exclusion chromatography (c) Protein-containing elution fractions concentrated for further analysis.

In the SDS-PAGE analysis, very thin bands around 42 kDa were observed for collected peak fractions (Figure 3.14-b). To enable a more accurate analysis of bands, the fractions corresponding to peaks were concentrated and run in the SDS-PAGE. In the concentrated fractions of peaks bands were observed at 42 kDa (Figure 3.14-c). These results demonstrate that the expressed ABL1 exists in different oligomeric states.

3.8. Crystallization and Co-crystallization Trials

Following the purification and concentration of ABL1, it is subjected to the apo and co-crystallization trials with both commercial TKIs, including Imatinib and Dasatinib, and novel hit compounds HT-A, Blg-AC, Dasa-Dtc, Bosu-A, MT-C, and HOA-1.

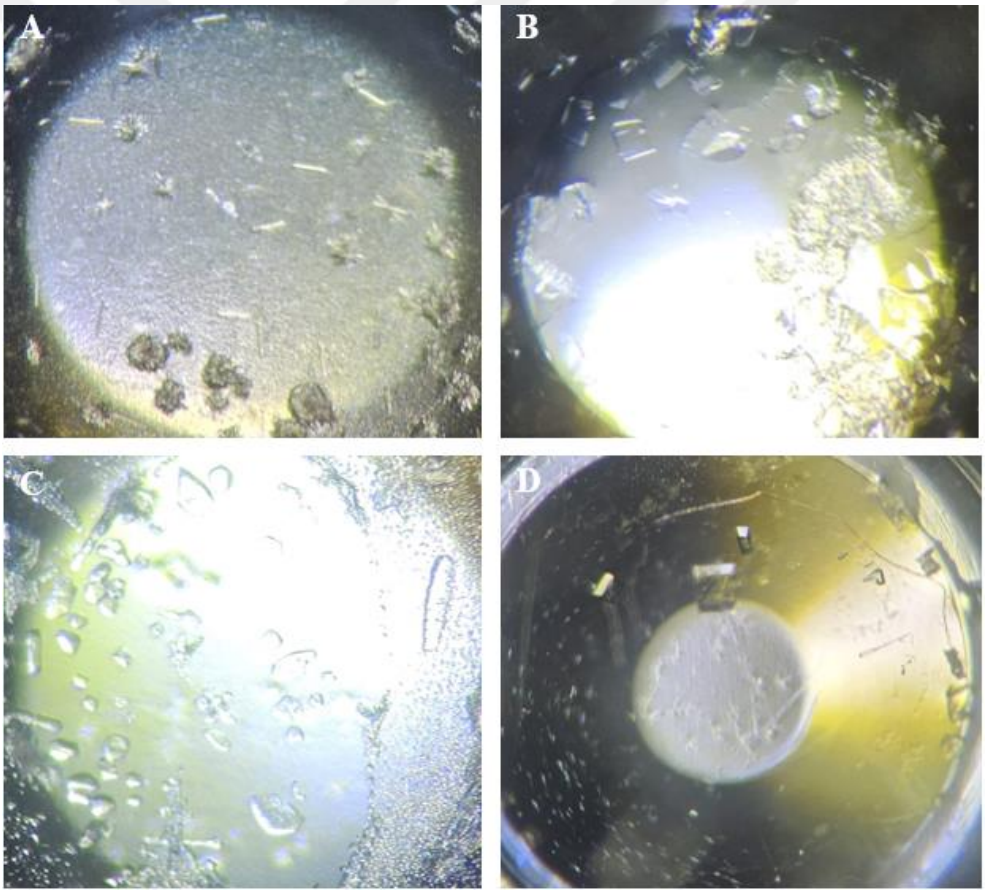

Figure 3.15: The crystals observed under the light microscope for the crystallization of ABL1 under conditions (a) Membrane Fac#45 (b) Index I #14 (c) Jena I #3 (d) Clear Strategy pH 6.5 #45

Among over 3500 screening conditions tested, including diverse buffers, precipitants, pH values, and additives, promising crystallization candidates were identified. While well-ordered protein crystals suitable for X-ray diffraction have yet to be obtained, the crystalline material observed under the microscope (Figure 3.15) was characterized as salt crystals based on their distinctive morphology and preliminary X-ray diffraction patterns (Figure 3.16). These findings provide valuable insights that will guide further optimization efforts toward successful protein crystal growth.

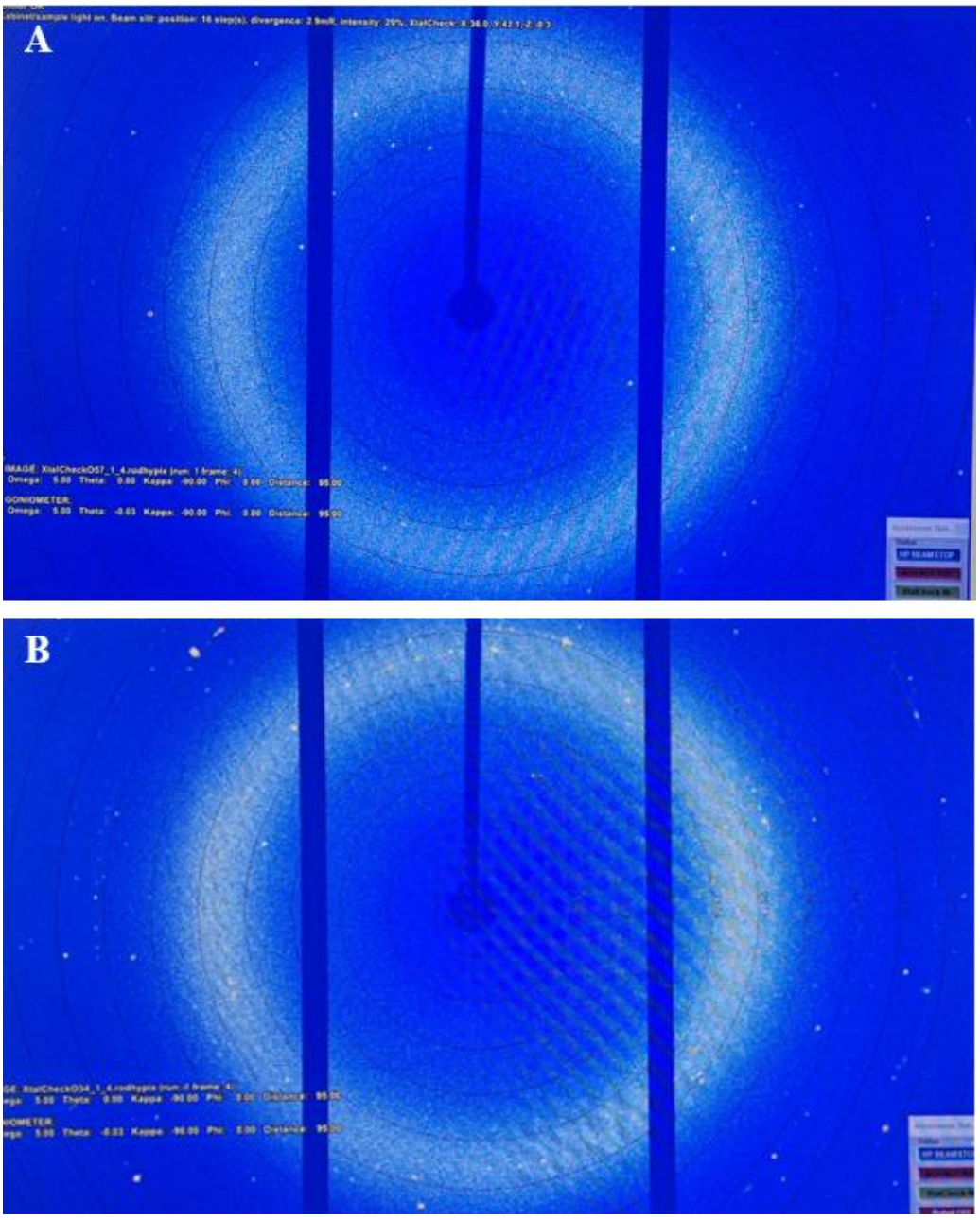

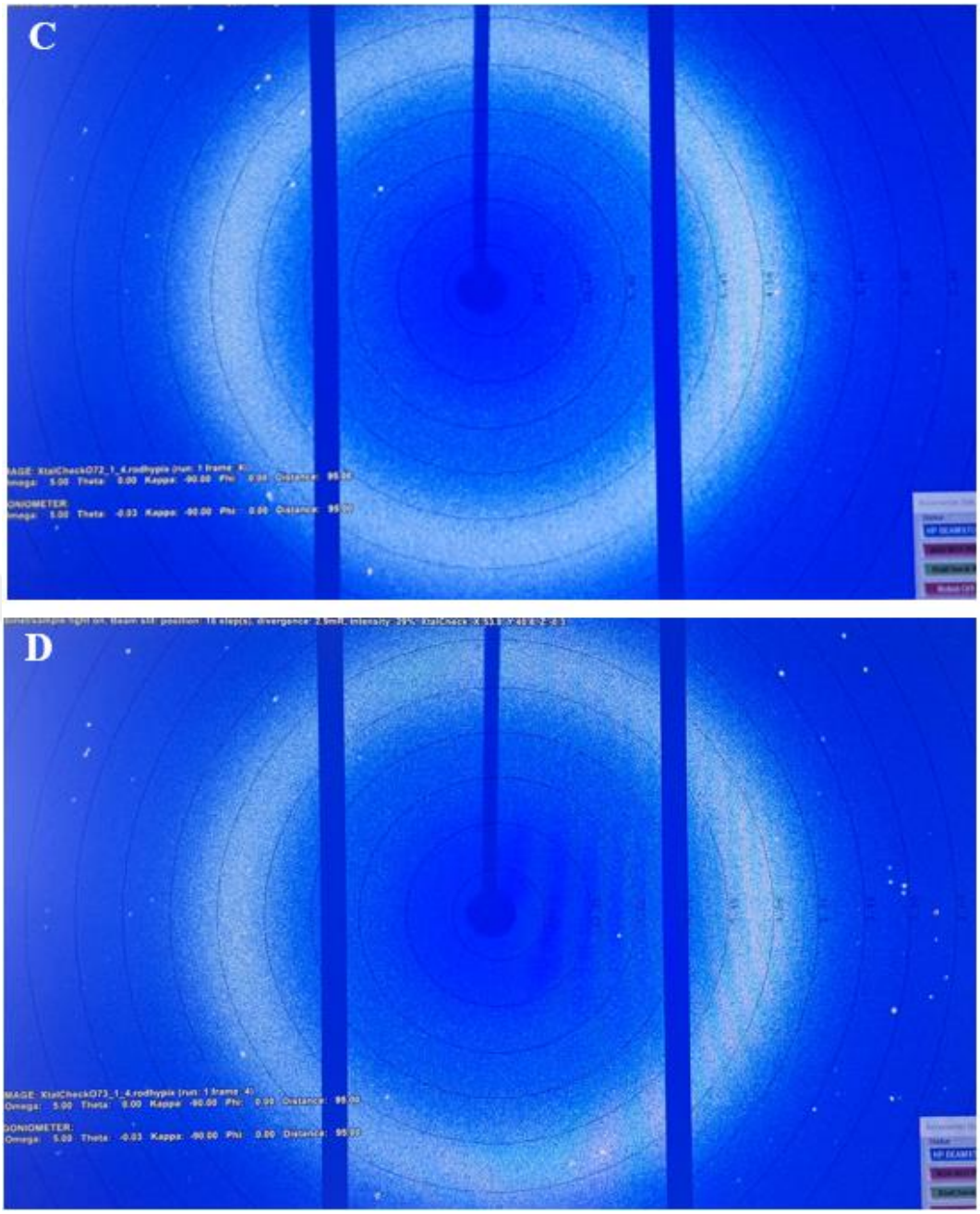

Figure 3.16: X-ray diffraction patterns of crystals observed under the conditions (a) Membrane Fac#45 (b) Index I #14 (c) Jena I #3 (d) Clear Strategy pH 6.5 #45

Chapter 4

DISCUSSIONS AND CONCLUSION

ABL1 is involved in various signaling pathways and plays a key role in several cellular processes. As a consequence of its crucial roles in the cell, its kinase activity is tightly controlled to maintain cellular homeostasis, and abnormal kinase activity is associated with disease pathogenesis, including CML. Dysregulated ABL1 activity is the main driver of CML, which makes ABL1 the primary target for the treatment approaches. TKI that targets the regulating abnormal ABL1 kinase activity have improved disease management for over 20 years. Despite their success in the treatment of the disease, novel TKIs and therapeutics are required to overcome the developed drug resistance and to improve the treatment efficiency.

At this point, structural studies aiming to enlighten the structural features of ABL1 have a fundamental role in the design and development of novel TKIs by providing knowledge on the potential target motifs and residues. Furthermore, structural studies by providing the atomic level information about the ABL1 can provide a deeper understanding of its functional role in the cell, kinase activity regulation, as well as its vital role in the pathogenesis of CML.

For the structural analysis of proteins via X-ray crystallography, the formation of high-quality crystals is necessary. The quality of the crystals is mainly dependent on the efficiency of the expression and purification steps, which determine the purity and concentration of the proteins. To enable high-quality protein crystals, a highly purified and concentrated protein is required, as a result of which sufficient expression and purification steps are required. In this study, the expression and purification of recombinant human ABL1 kinase domain, followed by the crystallization trials for further structural analysis via X-ray crystallography, were performed.

ABL1 has a structural diversity composed of several functional domains and motifs. Among various domains, the kinase domain is the primary target for structural studies, including this one, due to its role in disease progression and as the target of TKIs. For the recombinant expression of ABL1 kinase domain, the pET-28a(+) bacterial expression vector, including a 6X-His tag at the N-terminus, facilitating the purification of the protein via Ni-NTA affinity chromatography, was used. To enhance the protein solubility, a

SUMO tag was added to the N-terminus of the protein (Tao et al., 2018). In the mini-scale, the expression of recombinant human ABL1 kinase domain within *E. coli* BL21 Rosetta2^{TM} was successfully achieved. However, even with the addition of the SUMO-tag, the expressed proteins were observed in the pellet as aggregates rather than soluble fractions in the supernatant, indicating the tendency of ABL1 for aggregation and the requirement for further optimizations in the growth conditions.

First, for facilitating the protein expression, the induction conditions were optimized. Among the tested induction conditions, the highest level of protein expression was achieved by the induction with 0.4 mM IPTG at 18 °C overnight. Following the optimization of the induction conditions, the soluble expression of ABL1 was tested under the treatment with lysis buffers with varying compositions, including pH and salt concentration. However, any soluble protein fraction was achieved under the test of different pHs and salt concentrations.

Among the various tested conditions, soluble expression of ABL1 in the supernatant was achieved only under detergent treatment. In addition to the observation of soluble protein fractions both under urea and sarkosyl treatment, the bands at 42 kDa corresponding to ABL1 were observed in the pull-down samples, indicating the interaction of 6X-His-tagged ABL1 with Ni-NTA beads. These results suggest that both detergents effectively solubilized ABL1 inclusion body aggregates, enabling their interaction with Ni-NTA beads via the 6X-His tag. To enable the highest soluble protein expression, the detergent concentrations within the lysis buffers were optimized as 8M urea and %0.5 sarkosyl, respectively.

Following the achievement of the soluble expression of ABL1, its large-scale expression was performed separately under urea and sarkosyl treatments. Although both detergents yielded comparable results at the mini-scale, notable differences in purification efficiency emerged during large-scale expression and subsequent Ni-NTA affinity purification. In the purification followed by urea solubilization, the majority of the protein was observed in the flowthrough and wash steps, indicating the proteins flowed through the column instead of binding. Only a low amount of protein was eluted within two elution fractions. In the purification of ABL1, followed by its solubilization via sarkosyl, the protein bands were observed in several elution fractions compared to elution fractions of the purification followed by urea treatment. The requirement of the additional refolding step in the urea solubilization makes this approach more challenging and reduces its practicality compared to sarkosyl treatment. Sarkosyl solubilization offers a simpler and

more efficient alternative, enabling higher protein yield and concentration without the need for refolding (Fernandez-Soto et al., 2020).

The main limitation in the use of sarkosyl as a solubilizing agent is the challenges in the purification steps since it is not fully compatible with the Ni-NTA resin (Fernandez-Soto, 2020). To improve the purification efficiency and enhance the protein binding, the use of sarkosyl in low concentrations < %1 followed by dialysis was recommended (Tao et al., 2018, Fernandez-Soto et al., 2020). Despite the use of a low concentration of sarkosyl, %0.5, and applied dialysis still some of the protein did not bind to the column and flowed through in the flowthrough and Wash steps. A similar result was observed in the reverse chromatography, despite the uncut 6X-His-SUMO-tag, the protein flowed through instead of binding to the column. Additionally, another potential reason for the loss of the target protein in the flowthrough and wash steps is the insufficient resin capacity for binding of all the applied target protein (Novianti et al., 2024).

Following the ABL1 purification, 6X-His-SUMO tag cleavage trials were performed in the mini-scale. Among tested incubation temperatures, durations, and enzyme to protein ratios, the highest cleavage efficiency was observed at 4 °C incubation for 2 hours, 1:100 enzyme to protein ratio. After optimizing the enzymatic conditions in the mini-scale, the cleavage of the 6X-His-SUMO tag by ULP1 was performed on a large scale with the optimized reaction conditions. However, in a large-scale setting, any cleavage of the 6X-His-SUMO tag was not observed despite using identical buffer composition and incubation parameters. This unexpected result may be related to potential changes in the reaction parameters with the scaling-up to reaction volume (Pozdnyakov et al., 2022). In large-scale enzymatic reactions, dilution-related inactivation or uneven distribution of ULP1 protease can be observed. Furthermore, in large-scale reactions, enzyme diffusion and local concentration gradients can significantly impact the proteolytic activity of the ULP1.

In the SEC analysis of the purified ABL1, multiple peaks corresponding to 42 kDa bands in the SDS-PAGE were observed. These results demonstrated the protein heterogeneity with the presence of ABL1 in different oligomeric states. The protein heterogeneity observed in the SEC analysis has the potential to hinder the formation of high-quality crystals (Bhat, 2018). This conformational heterogeneity of ABL1 can pose a significant barrier to crystallization by preventing the formation of uniform, well-ordered crystals.

In addition to oligomeric heterogeneity, several potential factors that could complicate the crystallization of the ABL1 kinase domain were identified. While sarkosyl effectively solubilized inclusion bodies, its interaction with the protein may alter the protein's surface properties and disrupt critical intermolecular interactions necessary for the formation of a well-ordered crystal lattice. Furthermore, the SUMO tag, due to its inherent flexibility and size, can introduce conformational heterogeneity when not cleaved from the target protein. This flexibility can prevent the uniform packing of protein molecules within the crystal lattice by increasing structural disorder. As a result, the presence of the uncleaved SUMO tag may hinder the formation of well-ordered crystals (Bell et al., 2013). Another important factor is the structural flexibility and dynamic nature of the ABL1 kinase domain, which further complicates capturing a single, stable conformation suitable for crystallization (Holcomb et al., 2017).

Even though the efficient expression and purification of the protein, for the formation of well-ordered, high-quality crystals, the intrinsic properties of the protein, including conformational or oligomeric variability, also have to be considered. This underscore the challenges associated with crystallizing structurally heterogeneous and dynamic proteins.

Although protein crystals have not yet been obtained, the expression and purification processes of recombinant human ABL1 kinase domain have been successfully optimized at this stage of the study. Important data regarding the solubilization of ABL1 aggregates and protein heterogeneity have been gathered. These data play a critical role in guiding subsequent experiments and further structural biology studies.

As conclusion, in this study, the expression, solubilization, purification, and initial crystallization trials of the recombinant human ABL1 kinase domain were performed. Induction conditions were optimized using 0.4 mM IPTG induction at 18 °C overnight, which enhanced the yield of the protein expression. Insoluble fractions were effectively solubilized using urea and sarkosyl, enabling the recovery of aggregated ABL1. Sarkosyl was chosen over urea for protein solubilization due to its simplicitiy and higher efficiency over urea solubilization. The soluble ABL1 was purified via Ni-NTA affinity chromatography with minimum impurities. 6X-His-SUMO tag cleavage trials by ULP1 protease were also performed to obtain tag-free ABL1. In the performed SEC analysis, the oligomeric heterogentiy of the ABL1 was observed. Although crystals have not yet been obtained, this work has provided essential insights into the expression and production ABL1, for future structural and functional studies, particularly to development of novel TKI strategies.

BIBLIOGRAPHY

Bell, M. R., Engleka, M. J., Malik, A., & Strickler, J. E. (2013). To fuse or not to fuse: what is your purpose?. *Protein science : a publication of the Protein Society*, *22*(11), 1466–1477. https://doi.org/10.1002/pro.2356

Bhat, E. A., Abdalla, M., & Rather, I. A. (2018). Key factors for successful protein purification and crystallization. *Global Journal of Biotechnology and Biomaterial Science*, *4*(1), 1–7.

Chayen, N. E., & Saridakis, E. (2008). Protein crystallization: From purified protein to diffraction-quality crystal. *Nature Methods*, *5*(2), 147–153.

Deininger, M. W., Goldman, J. M., & Melo, J. V. (2000). The molecular biology of chronic myeloid leukemia. *Blood, The Journal of the American Society of Hematology*, *96*(10), 3343-3356.

El-Tanani, M., Nsairat, H., Matalka, I. I., Lee, Y. F., Rizzo, M., Aljabali, A. A., ... & Tambuwala, M. M. (2024). The impact of the BCR-ABL oncogene in the pathology and treatment of chronic myeloid leukemia. *Pathology-Research and Practice*, *254*, 155161.

Eshaq, A. M., Flanagan, T. W., Hassan, S. Y., Al Asheikh, S. A., Al-Amoudi, W. A., Santourlidis, S., ... & Hassan, M. (2024). Non-receptor tyrosine kinases: their structure and mechanistic role in tumor progression and resistance. *Cancers*, *16*(15), 2754.

Fernandez-Soto, P., Cavet, J. S., & Tabernero, L. (2020). Expression and purification of soluble recombinant SapM from *Mycobacterium tuberculosis*. *Protein Expression and Purification*, *174*, 105663.

Giegé, R., Lorber, B., & Théobald-Dietrich, A. (1994). Crystallogenesis of biological macromolecules: Facts and perspectives. *Acta Crystallographica Section D: Biological Crystallography*, *50*(Pt 4), 339–350.

Gul, M., Ayan, E., Destan, E., Johnson, J. A., Shafiei, A., Kepceo˘glu, A., ... DeMirci, H. (2023). Rapid and efficient ambient temperature X-ray crystal structure determination at Turkish Light Source. Scientific reports, 13(1), 8123.

Gutiérrez, D. A., Chandía-Cristi, A., Yáñez, M. J., Zanlungo, S., & Álvarez, A. R. (2023). c-Abl kinase at the crossroads of healthy synaptic remodeling and synaptic dysfunction in neurodegenerative diseases. *Neural Regeneration Research*, *18*(2), 237-243.

Hantschel, O., Nagar, B., Guettler, S., Kretzschmar, J., Dorey, K., Kuriyan, J., & Superti-Furga, G. (2003). A myristoyl/phosphotyrosine switch regulates c-Abl. *Cell*, *112*(6), 845-857.

Hari, S. B., Perera, B. G., Ranjitkar, P., Seeliger, M. A., & Maly, D. J. (2013). Conformation-selective inhibitors reveal differences in the activation and phosphate-binding loops of the tyrosine kinases Abl and Src. *ACS chemical biology*, *8*(12), 2734–2743.

Holcomb, J., Spellmon, N., Zhang, Y., Doughan, M., Li, C., & Yang, Z. (2017). Protein crystallization: Eluding the bottleneck of X-ray crystallography. *AIMS biophysics*, *4*(4), 557–575. https://doi.org/10.3934/biophy.2017.4.557

Irgit, A., Kamıs, R., Sever, B., Tuyun, A. F., Otsuka, M., Fujita, M., ... & Ciftci, H. (2025). Structure and dynamics of the ABL1 tyrosine kinase and its important role in chronic myeloid leukemia. *Archiv der Pharmazie*, *358*(5), e70005.

Jabbour, E., & Kantarjian, H. (2024). Chronic myeloid leukemia: 2025 update on diagnosis, therapy, and monitoring. *American journal of hematology*, *99*(11), 2191-2212.

Krishnan, K., Tian, H., Tao, P., & Verkhivker, G. M. (2022). Probing conformational landscapes and mechanisms of allosteric communication in the functional states of the ABL kinase domain using multiscale simulations and network-based mutational profiling of allosteric residue potentials. *The Journal of Chemical Physics*, *157*(24).

Levinson, N. M., & Boxer, S. G. (2012). Structural and spectroscopic analysis of the kinase inhibitor bosutinib and an isomer of bosutinib binding to the Abl tyrosine kinase domain. *PloS one*, *7*(4), e29828.

Levinson, N. M., Kuchment, O., Shen, K., Young, M. A., Koldobskiy, M., Karplus, M., Cole, P. A., & Kuriyan, J. (2006). A Src-like inactive conformation in the abl tyrosine kinase domain. *PLoS biology*, *4*(5), e144.

McPherson, A., & Gavira, J. A. (2014). Introduction to protein crystallization. *Acta Crystallographica Section F: Structural Biology Communications*, *70*(Pt 1), 2–20. https://doi.org/10.1107/S2053230X13033141

Minciacchi, V. R., Kumar, R., & Krause, D. S. (2021). Chronic myeloid leukemia: a model disease of the past, present and future. *Cells*, *10*(1), 117.

Mishra, S. K., Demo, G., Koča, J., & Wimmerová, M. (2012). In silico engineering of proteins that recognize small molecules. *IntechOpen*. https://doi.org/10.5772/36389

Novianti, M. T., Subroto, T., Efendi, Y. S., Baroroh, U., Kusumawardani, S., Gumilar, G., ... & Gaffar, S. (2024). Expression, Sarkosyl solubilization, DNase activity,

purification, and SPR binding affinity of recombinant diphtheria toxoid (rCRM197EK) expressed in *Escherichia coli* BL21 (DE3). *Molecular Biotechnology*, 1–11.

Oruganti, B., Lindahl, E., Yang, J., Amiri, W., Rahimullah, R., & Friedman, R. (2022). Allosteric enhancement of the BCR-Abl1 kinase inhibition activity of nilotinib by cobinding of asciminib. *Journal of Biological Chemistry*, *298*(8).

Paul, M. K., & Mukhopadhyay, A. K. (2004). Tyrosine kinase – role and significance in cancer. *International Journal of Medical Sciences, 1*(2), 101.

Pozdnyakov, N., Shilov, S., Lukin, A., & others. (2022). Investigation of enzymatic hydrolysis kinetics of soy protein isolate: Laboratory and semi-industrial scale. *Bioresources and Bioprocessing*, *9*, 37. https://doi.org/10.1186/s40643-022-00518-2

Roskoski Jr, R. (2022). Targeting BCR-Abl in the treatment of Philadelphia-chromosome positive chronic myelogenous leukemia. *Pharmacological Research*, *178*, 106156.

Rygiel, K. A., & Elkins, J. M. (2023). Recent advances in the structural biology of tyrosine kinases. *Current Opinion in Structural Biology, 82*, 102665.

Sacha, T. (2014). Imatinib in chronic myeloid leukemia: an overview. *Mediterranean journal of hematology and infectious diseases*, *6*(1), e2014007.

Sampaio, M. M., Santos, M. L. C., Marques, H. S., de Souza Gonçalves, V. L., Araújo, G. R. L., Lopes, L. W., ... & de Melo, F. F. (2021). Chronic myeloid leukemia-from the Philadelphia chromosome to specific target drugs: A literature review. *World journal of clinical oncology*, *12*(2), 69.

Sawyers, C. L. (1999). Chronic myeloid leukemia. *New England Journal of Medicine*, *340*(17), 1330-1340.

Shoukier, M., Kubiak, M., & Cortes, J. (2021). Review of new-generation tyrosine kinase inhibitors for chronic myeloid leukemia. *Current oncology reports*, *23*(8), 91.

Siveen, K. S., Prabhu, K. S., Achkar, I. W., et al. (2018). Role of non-receptor tyrosine kinases in hematological malignancies and its targeting by natural products. *Molecular Cancer, 17*, 31.

Smyth, M. S., & Martin, J. H. (2000). X-ray crystallography. *Molecular Pathology: MP*, *53*(1), 8–14. https://doi.org/10.1136/mp.53.1.8

Tanneeru, K., & Guruprasad, L. (2013). Ponatinib is a pan-BCR-ABL kinase inhibitor: MD simulations and SIE study. *PLoS One*, *8*(11), e78556.

Tao, H., Liu, W., Simmons, B. N., Harris, H. K., Cox, T. C., & Massiah, M. A. (2010). Purifying natively folded proteins from inclusion bodies using Sarkosyl, Triton X-100, and CHAPS. *BioTechniques*, *48*(1), 61–64. https://doi.org/10.2144/000113304

Weber, P. C. (1991). Physical principles of protein crystallization. *Advances in Protein Chemistry*, *41*, 1–36. https://doi.org/10.1016/s0065-3233(08)60196-5

Wu, A., Liu, X., Fruhstorfer, C., & Jiang, X. (2024). Clinical Insights into Structure, Regulation, and Targeting of ABL Kinases in Human Leukemia. *International Journal of Molecular Sciences*, *25*(6), 3307.

Xie, T., Saleh, T., Rossi, P., Miller, D., & Kalodimos, C. G. (2022). Imatinib can act as an Allosteric Activator of Abl Kinase. *Journal of molecular biology*, *434*(2), 167349.

Zhang, H., Zhu, M., Li, M., Ni, D., Wang, Y., Deng, L., ... & Cai, C. (2022). Mechanistic insights into co-administration of allosteric and orthosteric drugs to overcome drug-resistance in T315I BCR-ABL1. *Frontiers in Pharmacology*, *13*, 862504.

Appendix A:

CHEMICALS

Ampicillin	GOLDBIO
Chloramphenicol	GOLDBIO
Glycerol	ISOLAB
Imidazole	BioFroxx
IPTG	GOLDBIO
LB Agar	Caisson
NaCl	ISOLAB
HCl	ISOLAB
Ni-NTA	QIAGEN
Paraffin Oil	Tekkim Kimya
Sarkosyl	Sigma-Aldrich
SDS	Sigma-Aldrich
Tris Base	Sigma-Aldrich
Triton X-100	Sigma-Aldrich
Tryptone	BD Biosciences
Urea	ISOLAB
Yeast Extract	BD Biosciences

Appendix B:

EQUIPMENTS

AKTA Go Junior	Cytiva
AKTA	Cytiva
Beckman Allegra 15R Centrifuge	Beckman Coulter
Beckman Avanti J-26S	Beckman Coulter
Beckman OptimaTM L-80 XP Ultracentrifuge	Beckman Coulter
Beckman Ti-45 Rotor	Beckman Coulter
Branson W250 Sonifier	Branson
Cryotubes	Wuxi NEST Biotechnology
Eppendorf Tubes	Eppendorf New Brunswick
Falcon Tubes	FIRATMED
Innova 44R Incubator Shaker	Eppendorf New Brunswick
Innova 4430R Incubator Shaker	Eppendorf New Brunswick
Kimtech Science KimWipes	Kimberly-Clark
NanoDrop™ 2000c	Thermo Scientific
Terasaki Plates	Greiner Bio-One
TGX-Mini Protean Gradient SDS-PAGE System	Bio-Rad Laboratories
Bio-Rad Laboratories	Merck Millipore
Rigaku XtaLAB Synergy Flow XRD	Rigaku
Superdex™200 Increase Column	Cytiva

Appendix C:

PROTEIN LADDER

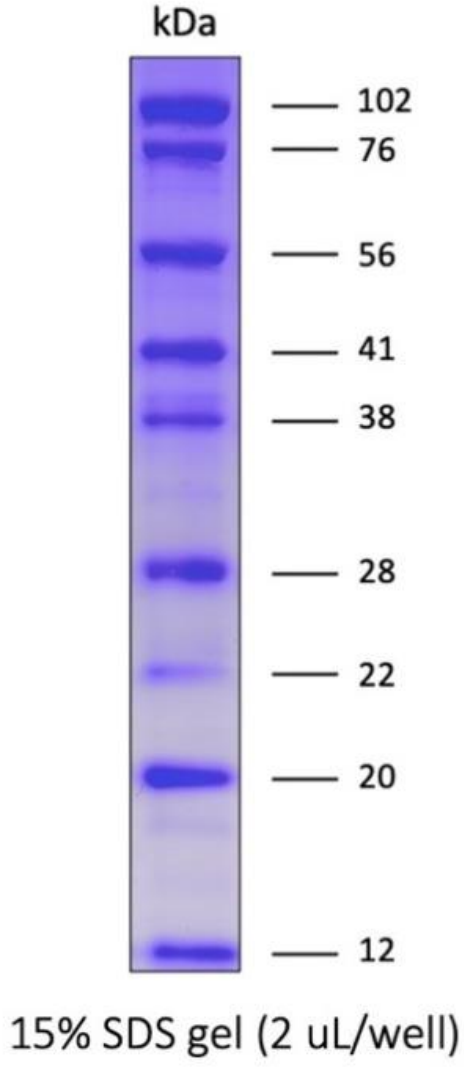

Figure C.1: KUYBIIG-M Protein Ladder.

Appendix D:

CRYSTALLIZATION SCREENING CONDITIONS

3D Structure Screen	Molecular Dimensions
Additive Screen	Hampton Research
Clear Strategy Screen	Molecular Dimensions
CryoPro	Hampton Research
Crystal Screen	Hampton Research
Crystal Screen Cryo	Hampton Research
Detergent Screen	Hampton Research
Grid Screen Ammonium Sulfate	Hampton Research
Grid Screen MPD	Hampton Research
Grid Screen PEG/LiCl	Hampton Research
Grid Screen PEG6000	Hampton Research
Grid Screen Sodium Chloride	Hampton Research
Helix	Molecular Dimensions
Index	Hampton Research
Ionic Liquid Scree	Hampton Research
JBScreen Nuc-Pro	Jena Bioscience
JCSG	Molecular Dimensions
MacroSol	Molecular Dimensions
MembFac	Hampton Research
MIDAS	Molecular Dimensions
Morpheus	Molecular Dimensions
MultiXtal	Molecular Dimensions
Natrix	Hampton Research
NeXtal Protein Complex Suite	NeXtal Biotechnologies
NR-LBD	Molecular Dimensions
PACT Premier	Molecular Dimensions
PEG/Ion	Hampton Research
PEGRx	Hampton Research
PGA Screen	Molecular Dimensions
ProPlex Screen	Molecular Dimensions

Quick Screen	Hampton Research
SaltRx	Hampton Research
Structure Screen	Molecular Dimensions
Stura FootPrint Screen	Molecular Dimensions
Wizard	Rigaku
Wizard Cryo	Rigaku
Wizard Precipitant Synergy	Rigaku